AD 269 285

DISCLAIMER NOTICE

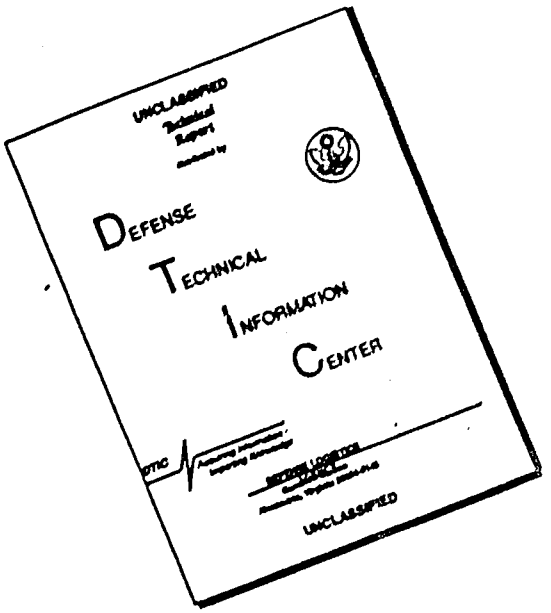

THIS DOCUMENT IS BEST QUALITY AVAILABLE. THE COPY FURNISHED TO DTIC CONTAINED A SIGNIFICANT NUMBER OF PAGES WHICH DO NOT REPRODUCE LEGIBLY.

U.S. AIR FORCE

Project RAND

RESEARCH MEMORANDUM

This is a working paper. It may be expanded, modified, or withdrawn at any time. The views, conclusions, and recommendations expressed herein do not necessarily reflect the official views or policies of the United States Air Force.

The RAND Corporation
SANTA MONICA • CALIFORNIA

U. S. AIR FORCE

PROJECT RAND

RESEARCH MEMORANDUM

THEORY OF IONIZED TRAILS FOR BODIES AT HYPERSONIC SPEEDS

Paul S. Lykoudis*

RM-2682-1-PR

May 29, 1961
Revised October 5, 1961

Assigned to _____

This research is sponsored by the United States Air Force under contract No. AF 49(638)-700 monitored by the Directorate of Development Planning, Deputy Chief of Staff, Research and Technology, Hq USAF.

*Consultant, The RAND Corporation

The RAND Corporation
1700 MAIN ST. • SANTA MONICA • CALIFORNIA

SUMMARY

This report discusses the characteristics of the gaseous trail remaining behind a body moving through the atmosphere at hypersonic speeds. The purpose of this study of the hypersonic trail is the development of means for ascertaining those variables that can be measured and used to predict the characteristics of the body causing the trail, essentially its shape and weight.

The available theoretical and experimental literature is reviewed and the basic aspects of hypersonic trails are presented. In the case of thermodynamic equilibrium, a universal solution is found for the velocity and enthalpy distributions at a station behind the body where the pressure has reached its ambient free-stream value. This solution is given in terms of the coordinate defining the shape of the bow shock wave. It is found that the nondimensional velocity and enthalpy profiles depend strongly on the drag coefficient alone. These analytical results are in good agreement with available numerical solutions by the method of characteristics.

The thermal-conduction part of the trail is also studied. An analytic solution is found for the case of variable thermal conductivity. The length of the trail based on a minimum ionization level is calculated at different altitudes for an illustrative re-entry. It is shown that to within a good approximation this length is directly proportional to the local atmospheric density, to the drag coefficient, and to the object's cross-sectional area, for a constant flight velocity and for a relatively blunt body with boundary layer effects neglected. The influence of the trailing shock on the conduction part of the trail is discussed. A preliminary study is also made of the trail under chemically frozen conditions.

ACKNOWLEDGMENTS

The author wishes to express his sincere appreciation to Carl Gazley, Jr. for his enthusiasm, keen interest, discussions, and several contributions in reading the manuscript; he also wishes to thank the following persons whose kind cooperation, interest, and discussions helped in the writing of this memorandum: Saul Feldman (Electro-Optical Systems, Inc.), F. R. Gilmore (The RAND Corporation), M. Goulard (The Bendix Corporation), R. Goulard (The Bendix Corporation), Joseph Gross (The RAND Corporation), L. Hromas (Space Technology Laboratories), T. Y. Li (Rensselaer Polytechnic Institute), M. Rodriguez (Space Technology Laboratories), Mary Romig (The RAND Corporation), and R. Schamberg (The RAND Corporation).

CONTENTS

SYMBOLS

C_D = drag coefficient (forebody form drag)

C_p = specific heat at constant pressure

D = diffusion coefficient

d = diameter

E = electric field intensity

f = velocity ratio defined in Eq. (15)

h = enthalpy

$\bar{h}$ = nondimensional enthalpy defined in Eq. (6)

J,K = Bessel functions

k = coefficient of proportionality defined in Eq. (3)

k_t = thermal conductivity

L = length of trail

M = Mach number

m = mass, or exponent as defined in Eq. (3)

N = concentration of a species

Pr = Prandtl number

p = pressure

Re = Reynolds number

$R(x)$ = function defining bow shock wave

R_H = Howarth variable defined in Eq. (14)

r = radial distance of a streamline defined in Fig. 1

S = entropy

T = temperature

t = time

U = velocity in the axial direction

X = distance defined in Eq. (31)

x = axial distance

GREEK SYMBOLS

$\alpha(x)$ = nondimensional enthalpy at the axis defined in Eq. (34)

α' = numerical coefficient given in Ref. 18

β = Gaussian depth defined in Eq. (18)

β' = Gaussian depth defined in Eq. (34)

γ = ratio of specific heats

γ' = numerical coefficient given in Ref. 18

γ_L = equivalent ratio of specific heats defined in Eq. (7)

δ = effective thickness of conduction part of trail

δ_b = boundary-layer thickness

δ_s = shock-wave angle (see Fig. 1)

δ_w = characteristic thickness of the wake

ξ = electron attachment coefficient

μ = mobility or viscosity

ρ = density

ω = exponent

SUBSCRIPTS

E = corresponds to equilibrium flow

F = corresponds to frozen flow

s = corresponds to stagnation condition

x_o = distance as given by Fig. 1

∞ = corresponds to the free stream

I. INTRODUCTION

Trails of bodies moving at hypersonic speeds are of interest to meteor physicists and those concerned with the problems of describing man-made objects re-entering the earth's dense atmosphere.

Several papers have appeared recently that attempt to give an account of the different phenomena involved in the production of the trail and their possible use in predicting the geometry and flight characteristics of the object causing it. For those interested in acquiring a knowledge of the fundamental behavior of hypersonic trails under different flow regimes, a paper by Feldman offers an excellent introduction.(1)

Figure 1 depicts the different regions of the flow around a blunt body. The free-stream region is denoted by A; B is the subsonic region behind the strong part of the shock wave; C corresponds to the inviscid region between the bow shock wave and the trailing shock. The boundary layer over the body is denoted by E, whereas the "near wake" is shown as region F. The part of the flow that is shed behind the body by passing through the boundary layer forms an inner core, G, which will be referred to here as the wake. After expanding in region C, the flow is recompressed through the trailing shock entering region D in order to be re-expanded, this time in the direction of flow x. At a station $x = x_o$ the pressure will have reached the free-stream value and, from there on, thermal conduction and other transport mechanisms will determine the rate of the energy diffusion. This last region, H, is normally much longer than the distance x_o and forms what we shall call the trail. To summarize, viscous and heat-conducting effects are prominent in regions E, F, and G. Regions B, C, and D are considered

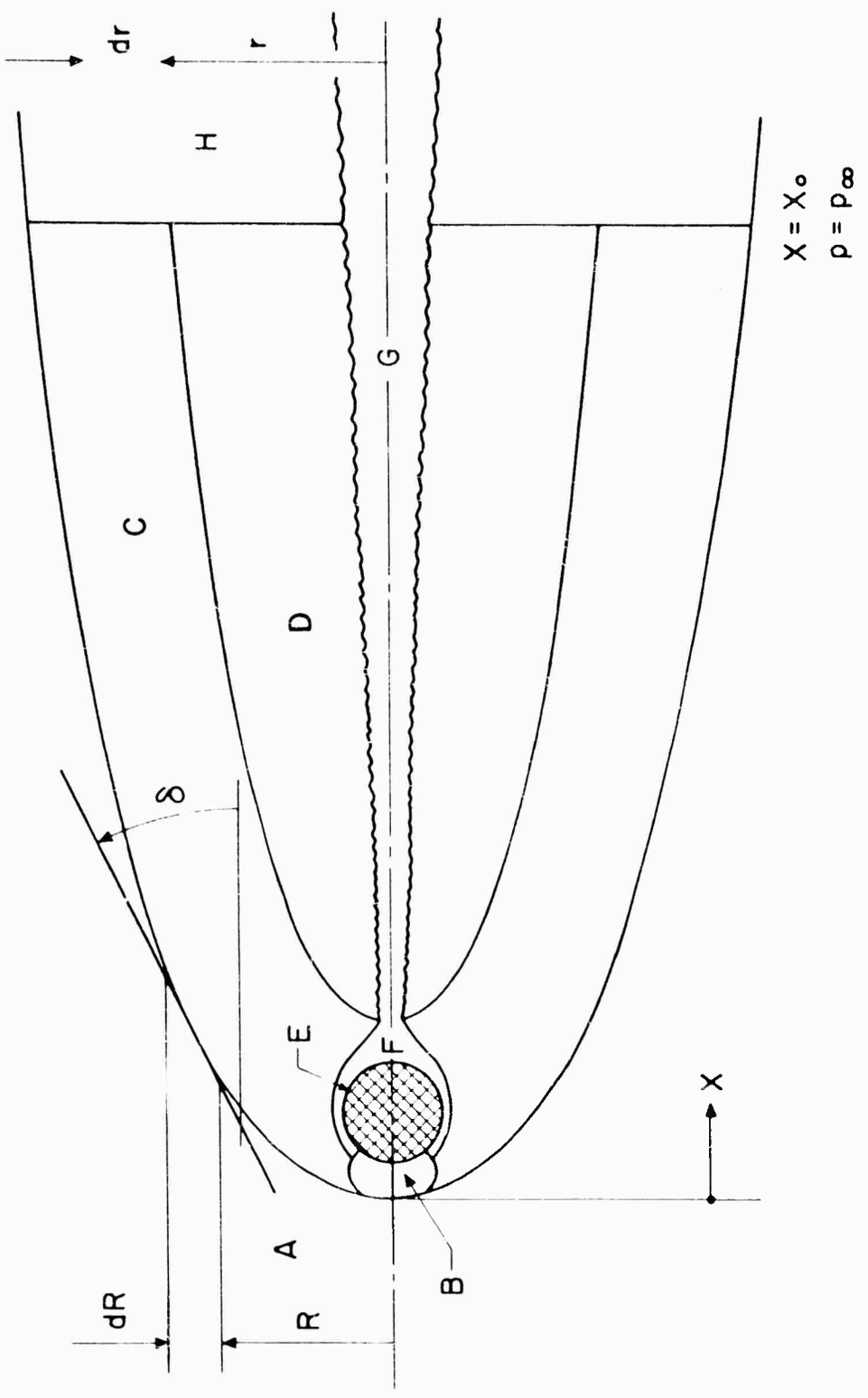

Fig. 1 — Characteristic regions of a hypersonic trail

inviscid and adiabatic, whereas in region H viscous effects are negligible compared to conduction.

The picture just given refers to a blunt body for which the trail is essentially the result of the large entropy generation created by the detached shock wave. It is obvious that slender pointed bodies, producing weaker shocks, will produce fewer thermodynamic observables in the trail. In the blunt geometry, the exact shape of the afterbody is not expected to influence appreciably the characteristics of the flow in the trail. The validity of this statement hinges essentially around the degree of irreversibility created by the trailing shock; inasmuch as sharply closing streamlines are not expected to form behind the body, the discontinuity due to the second shock may be assumed reversible on a first approximation. This point will be elaborated later.

As a first rough approximation, the trail will depend on the following parameters: altitude, velocity, and a characteristic length. The following a priori qualitative observations regarding the nature of the trail are based on general aerodynamic and thermodynamic arguments. At low altitudes, where the density is fairly high, we expect the flow to be in thermodynamic equilibrium everywhere. We also expect that the boundary-layer thickness around the body will be small and that, as a result, a small percentage of the energy associated with the flow will go through the boundary layer. In consequence, the viscous wake G is expected to be thin with a low energy content compared to the total energy. In such a case, we may neglect the existence of regions E, F, and G (see Fig. 1).

Consider now the possibility of turbulence. It seems that low critical Reynolds numbers are needed in order for the viscous wake G to become unstable. The influence of turbulence on the observables in the

trail will be more important at those altitudes where more energy will be associated with a thicker boundary layer. On the other hand, the effect of region G, even though turbulent, will be minimized if its rate of growth in the radial direction is small. We conclude that at low altitudes, with a thin boundary layer, only the shape of the induced detached shock will determine the nature of the trail, and that knowledge of this shape should be adequate for the description of the trail.

At high altitudes, where the density is low, relaxation effects will be important. In the subsonic region B, where the densities are high due to the normal character of the shock, the flow will be dissociated, but in thermodynamic equilibrium. As the flow expands to lower densities the process of recombination of the dissociated species lags behind, since it is governed by a three-body collision; nonequilibrium effects then become important. In this case, the degree of departure from equilibrium will be governed not only by the local state of the fluid, but also by a characteristic length. For the same velocity, smaller lengths will be traveled at shorter times and, hence, a smaller number of collisions will be associated with the motion of the particles, resulting in larger departures from equilibrium. The phenomenon becomes more complicated when the rate of recombination of some species is different from that of others (for instance, atom-atom recombination versus ion-electron).

In the final analysis, refinement of the calculations will depend on the nature of the observable. For instance, if observation of a trail in thermodynamic equilibrium is planned with a radar beam, the electron-concentration profiles are of importance; some error in the prediction of the thermodynamic state (essentially temperature) can be tolerated.

On the other hand, if the radiant intensity of the trail is of interest, then because of the stronger dependence of radiation on temperature, a small error in temperature may lead to a manifold error.(1) In this connection it should be emphasized that the definition of the trail length depends on the nature of the observable and on the observing instrumentation. For a chosen observable, the trail length may be defined as the distance behind the body at which a given instrument is unable to discriminate or record from ambient conditions.

Chemical relaxation effects become important above an altitude of about 100,000 ft for objects of reasonable size re-entering at satellite or ICBM velocity. At an altitude roughly above 300,000 ft, most of the diatomic particles are absent, and mean-free-path effects become important. Coupling effects in the ionosphere with the earth's magnetic field are possible, but this region has yet to be studied in a systematic way. It is obvious, nevertheless, that the observables are no longer associated with the existence of an entropy trail in the sense described in this section.

A study of the hypersonic trail aims at the development of thermodynamic profiles of those parameters which, with our present state of knowledge, can be measured. These measurements are used in an attempt to predict the characteristics of the body causing the trail, essentially its shape and weight.

II. DISCUSSION OF AVAILABLE RESULTS

THE TRAIL IN THERMODYNAMIC EQUILIBRIUM

For the reasons enumerated in the previous section, low altitudes will be associated with thermodynamic equilibrium; furthermore, the role of viscosity, confined to regions E, F, and G (see Fig. 1) will be relatively small.

Assuming that the amount of fluid entering the region G is equal to the fluid mass going through the boundary layer over the body, we have the following order-of-magnitude equality:

$$\rho\delta_w^2 U \sim \rho\delta_b r_o U$$

Here δ_w is the characteristic thickness of the wake G and δ_b the boundary-layer thickness over the body. We conclude that

$$\delta_w/r_o \sim \sqrt{\delta_b/r_o}$$

This means that as long as δ_b remains small, δ_w will also be small. The same argument was offered in Ref. 1.

The calculation of the trail proceeds in the following way. For given geometry and flight conditions, we calculate the shape of the shock wave and the inviscid flow behind it by making use of the method of characteristics. We will start with a blunt nose and consider different afterbodies and trailing conditions. Feldman[1,2] has investigated the case of a two-dimensional blunt nose followed by a flare of an angle between 0 and 30 deg and by an expansion in the near-wake region F between 0 and 20 deg. These calculations were carried out for both a short and a long body. Similar calculations have been carried out for a hemisphere followed by a frustum,

or a true streamline and then a cylinder.* Frustum or free-streamline angles up to 30 deg were considered. All of the above results indicate that at a distance of about 10 radii behind the body, the thermodynamic state is very nearly the same as the one corresponding to an isentropic flow for expansion angles up to 20 deg. A difference in temperature of about 10 per cent was found for a frustum of 30 deg, but it should be recognized that this is an extreme case not to be anticipated in reality. An expansion angle of 20 deg is supported by available experimental evidence.** The effect of the exact geometry of the afterbody on the equilibrium electron concentration and radiation emitted in the optical ($\cong$ 2,000 A^{o} to 10,000 A^{o}) and infrared ($\cong$ 5.3 microns) region of the spectrum has been evaluated in Ref. 1. The final conclusion is

> ... [the] magnitude of thermal radiation and electron density that are arrived at on the basis of calculations of a simple blunt body geometry like a hemisphere-cylinder, that does not include the geometrical details of the afterbody, may be off by a factor of not more than 3.

Since the reflecting qualities of a radar beam over an ionized trail depend on its plasma frequency, which is directly proportional to the square root of the electron concentration, the error in the plasma frequency is diminished. In this memorandum, the problem of interaction between a radar beam generating a field E varying as $\exp(i\kappa x + i\omega_R t)$ and a medium containing N_e electrons/cm^3 will not be covered. The following

---

*Personal communication with L. Hromas, Space Technology Laboratories, Inc.

**This expansion angle is eventually determined by consideration of viscous effects. No theoretical work seems to be available at present in this region.

simple notions could be useful, however. The wave equation in which E_y is propagated in the x axis is

$$\frac{\partial^2 E_y}{\partial x^2} - \frac{4\pi N_e e^2}{m_e c^2} \frac{\partial E_y}{\partial t} = \frac{1}{c^2} \frac{\partial^2 E_y}{\partial t^2}$$

The phase velocity V is given as follows

$$V^2 = \frac{c^2}{1 - \omega_p^2/\omega_R^2}$$

where

$$\omega_p = \text{plasma frequency} = \left(\frac{4\pi N_e e^2}{m_e} \right)^{1/2}$$

or

$$\frac{\omega_p}{2\pi} = 8.97 \times 10^3 \, N_e^{1/2} \approx 10^4 \sqrt{N_e} \quad \text{cycles/sec}$$

For $\omega_p > \omega_R$ the signal ω_R is reflected, whereas for $\omega_p < \omega_R$ the radar wave is damped out. The electron densities occurring in the ionosphere are of the order of 10^6 electrons/cm^3. It follows that no trail with a lower electron concentration can be detected by a radar beam.

Having established the reversible character of the geometry behind the blunt nose, the inviscid calculation is performed over a

hemispherc-cylinder configuration. Feldman[1,2] gives all the thermodynamic profiles for a hemisphere-cylinder geometry extending to the station $x = x_o$ of Fig. 1 where the pressure everywhere has reached approximately its free-stream value. For an altitude of 60,000 ft and velocity of 17,500 ft/sec the pressure reaches its free-stream value at a distance of about 56 radii.[1] For an altitude of 100,000 ft and velocities of 15,000, 20,000, and 25,000 ft/sec, the distances are about 40, 80, and 100 radii, respectively.* In all cases, this is a small fraction of the total length of the trail over which temperature and electron-concentration gradients will persist.

As was stated in the previous section, from the station $x = x_o$ onwards, the trail will cool off after termination of the adiabatic expansion by the mechanism of heat conduction. Viscous dissipation offers a very small contribution, since thc velocity deficiency at the station $x = x_o$ at the center line is of the order of 20 per cent of the free-stream value. Solutions for the conduction-controlled part of the trail are available in Refs. 1 - 6.

In Ref. 1, the initial enthalpy and velocity profiles found by the method of characterristics and corresponding to the station $x = x_o$ are approximated by a Gaussian distribution of the form $e^{-R_H^2/\beta}$ where R_H is related to the physical radius r through the Howarth transformation

$$R_H^2 = 2\int_o^r \frac{\rho}{\rho_\infty}\, rdr$$

*Personal communication with S. Feldman, Electro-Optical Systems, Inc.

For this purpose, since all the characteristic profiles are calculated at the surface of the cylinder, the value at $r = r_o$ was transferred to $r = 0$ and the interval between the center line and $r = r_o$ was faired with a smooth curve. For the evolution of the trail during its thermal mixing, an integral method was applied, satisfying the exact boundary conditions and differential equation at $r \to 0$, and also the condition that the total energy and momentum in the radial direction extended to infinity remain constant at all stations x. From the final solution, it was found that the error made by neglecting the transfer of momentum in detail was very small. After the thermodynamic state inside the trail was thus established, calculations were made of electron-concentration profiles. The decay of infrared and optical radiation was also calculated along the axial streamline. The results are given for altitudes of 100,000 and 250,000 ft with velocities ranging between 15,000 and 35,000 ft/sec.

In Ref. 3 a solution of the conduction-controlled trail is offered, the equations of conservation being solved by the method of finite differences with the help of a digital computer. A comparison with Feldman's integral method[1] showed that the trail lengths based on electron-concentration profiles were about half the length of those obtained by the finite-difference method. This discrepancy has been attributed in Ref. 3 partly to the fact that the Gaussian initial profiles chosen by Feldman did not fit away from the axis when compared with those he obtained by the method of characteristics (see Fig. 2). Actually, comparison of the initial profile chosen by the Goulards in the physical plane[3] with the ones obtained by Feldman[1] shows that the discrepancy is due to a presumably erroneous interpolation in Ref. 3 between the

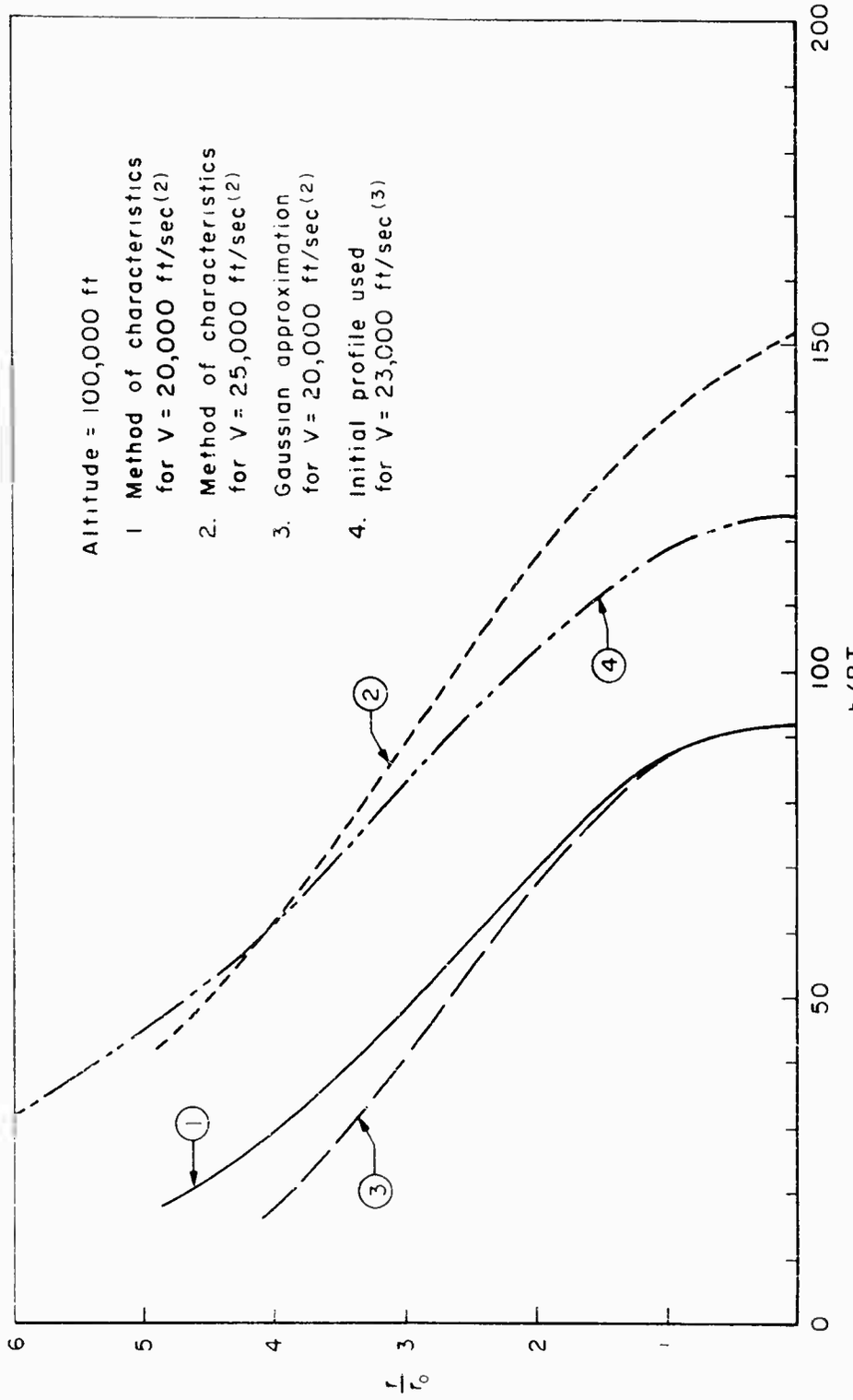

Fig. 2 — Comparison of initial enthalpy profiles before thermal mixing

velocities of 20,000 and 25,000 ft/sec. Inspection of Fig. 2 shows that Feldman's predictions of the trail length should be closer to the accurate ones. Furthermore, the findings reported in Section III will theoretically justify Feldman's choice of the Gaussian widths for his solution.

An equilibrium solution for a blunt body for an entropy-induced shock wave is also presented in Ref. 4. The initial velocity profile corresponding to the section $x = x_o$ is calculated by the streamtube method, starting with a known shock-wave shape and using real-gas tables for the isentropic expansion behind the body. The velocity profile found is highly irregular, and the authors approximate it by using the method of least squares with a third-degree polynomial, exhibiting the same behavior as a Gaussian distribution. The deviations from this approximation are large but no explanation of the reason is offered in the paper. A momentum-integral method is then used for the study of the trail. The enthalpy is calculated from the Crocco integral, the Prandtl and Lewis numbers both being assumed equal to unity. The electron concentration is given along the center line for an altitude of 200,000 ft and a velocity of 23,000 ft/sec.

RELAXATION EFFECTS

At present there is no definitive quantitative analysis available in the literature on nonequilibrium effects, apart from some preliminary calculations.

In Ref. 7 a study is made of the importance of relaxation effects along the stagnation streamline over a blunt configuration. Flight velocities of 15,000 and 25,000 ft/sec with altitudes between 154,000 and 246,000 ft have been considered. The major conclusion is that for altitudes

higher than 150,000 ft the flow in the inviscid supersonic expansion region of a blunt body will be essentially chemically frozen. It should be kept in mind that the transition to frozen conditions progresses very rapidly.[8] A thorough calculation of the whole inviscid field should, of course, include a study of all the streamlines crossing the bow shock wave.

In Ref. 3, it was found that transition to frozen flow develops at about 45 deg aft of the stagnation point for a velocity of 23,000 ft/sec, an altitude of 100,000 ft, and a characteristic length of 1 ft. It was also calculated that for the same flight velocity and same body diameter the transition point moves closer to the stagnation region at higher altitudes. For a velocity of 23,000 ft/sec and a radius of 1 ft, transition is almost at the stagnation point for altitudes above 150,000 ft. This means that above these altitudes the calculation could be simplified by assuming frozen conditions almost immediately behind the shock wave. It should be added that this procedure will be more correct for the streamlines closer to the stagnation region where most of the irreversibility (and interest) lies.

As a first approximation for the calculation of the temperature profile at the region $x = x_o$, on the assumption of complete frozen conditions, one could use the equivalent effective-specific-heat ratio for frozen air as given in Ref. 9 or 10. In general, this effective value approaches the ratio of 5/3 of a monatomic gas. The temperature at the axial streamline at the station $x = x_o$ would be lower if transition to frozen conditions occurred earlier. This is self-evident since the isentropic expansion at a higher value of γ_F takes place over a greater length of time. On the other hand, we expect to find, for the same body diameter and altitude, smaller dependence of the temperature at the station $x = x_o$ on the flight

velocity, as transition moves to the stagnation point. This may be understood as follows: The value of γ_F is higher for higher compressibility factors which, in turn, are higher for higher flight velocities or flight Mach numbers.(11) Since

$$T_{x_o} \sim T_s \left(\frac{p_\infty}{p_s}\right)^{\gamma_F - 1/\gamma_F} \sim M_\infty^{2/\gamma_F}$$

the increases in M_∞ will be moderated by decreases in the ratio $2/\gamma_F$. These qualitative remarks are substantiated by the calculations in Ref. 1, undertaken for an altitude of 200,000 ft and flight velocities between 10,000 and 30,000 ft/sec (see Fig. 7 of Ref. 1).

The variation of the electron concentration behind the body will next be considered. The rate of recombination of the ions with electrons is of primary importance here. It is evident that slower ion-electron recombination (high altitudes) will result in an electron concentration behind the body that is higher than the concentrations obtained for thermodynamic equilibrium. Nevertheless, at intermediate altitudes, with slow atom-atom recombination and fast ionic recombination, it is conceivable that lower-than-equilibrium electron concentrations may result, since under these conditions the electron density will be in equilibrium with the local frozen temperature (which is lower than the equilibrium temperature). This was pointed out first by S. C. Lin.(1)

Frozen-flow calculations of electron concentrations along the axis of the trail are also reported in Ref. 4. Again, as in the equilibrium calculations, all the profiles at $x = x_o$ computed by assuming frozen conditions immediately behind the shock wave were highly irregular. For

fitting, third-degree polynomials were used. The study consists essentially in a conservation and redistribution of the electron concentration in the trail. The exact thermochemistry of the phenomenon is not taken into account.

A summary of the work of Bortner is given in Ref. 5. Dissociation and ionization reactions have been taken into account. It is reported that an order-of-magnitude change in the oxygen-dissociation-rate constant can cause increases by factors of over 100 in the electron density. A 10-deg spherically blunted cone at an altitude of 160,000 ft is considered. The study is made along the stagnation streamline. It is found that the electron concentration six characteristic lengths behind the body is one order of magnitude higher if the flow is frozen. On the other hand, lower-than-equilibrium electron concentrations are predicted for mixed nonequilibrium flow. (This is the trend anticipated in Ref. 1 and discussed above.) A study is also made of contamination effects in the electron concentration. Equilibrium is assumed and contamination of one part sodium atoms per million and one part sodium atoms per ten thousand parts of equilibrium air is considered. The electron concentration is increased by at least three orders of magnitude for the altitude of 250,000 ft and Mach number 24. All of the above calculations extend to a few characteristic lengths behind the body in the inviscid region and do not cover the trail proper (region H of Fig. 1).

At rather high altitudes, where low densities prevail, the mechanism of ambipolar diffusion is of importance. This mechanism occurs because the rate of diffusion of the ions and electrons in the gas is different, thus causing a space-charge field. Consideration of the particular law of

motion for every species is difficult; nevertheless, a "gross" approach is traditionally used. We assume that the ion and electron concentrations remain the same and that their average velocities are equal. With the subscripts i and e corresponding to ions and electrons, and under the assumption that the gross space charge is represented by an electric field of magnitude E, we write

$$N_i \overline{v_i} = -D_i \frac{dN_i}{dx} + N_i \mu_i E$$

$$N_e \overline{v_e} = -D_e \frac{dN_e}{dx} - N_e \mu_e E$$

This is a charge-conservation equation for the motion in direction x. The first term on the right represents the diffusion contribution, whereas the second one gives the contribution from a velocity imparted to the particle by the presence of the space charge represented by E. This velocity is proportional to the mobility. Eliminating E from the above two equations by making $N_e = N_i = N$, $\overline{v_i} = \overline{v_e} = \bar{v}$, we have

$$N \bar{v} = -\left(\frac{D_e \mu_i + D_i \mu_e}{\mu_e + \mu_e} \right) \frac{dN}{dx}$$

which defines the "coefficient of ambipolar diffusion" D_a as

$$D_a = \frac{D_e \mu_e + D_i \mu_e}{\mu_i + \mu_e}$$

Simple kinetic theory shows that, irrespective of the difference of mass, $D_e/\mu_e \approx D_i/\mu_e \approx kT/e$, where k is Boltzmann's constant; taking into account the fact that $\mu_e >> \mu_i$, we find

$$D_a \approx 2D_i$$

Another mechanism, important under a wide range of conditions, is the attachment of electrons to neutral species, thus creating negative ions; in the case of air, this would involve the attachment of electrons to diatomic oxygen. The rate of attachment is proportional to the density of the electron and to the square of air-molecule density.

The electric-charge-continuity equation takes the form

$$-\frac{\partial N}{\partial t} = \zeta N N_a^2 + a_r N^2 - D_a \nabla^2 N$$

The first term on the right is the contribution through attachment, the second through recombination, and the third through ambipolar diffusion; N_a is the air-molecule density.

The mechanisms of ambipolar diffusion, recombination, and attachment are considered in some detail in Ref. 12. The computations are performed for a 5-in. re-entry body. Temperature variations in the reaction-rate coefficients have been neglected, since the variations in density with altitude are much more important. It is found that recombination prevails over ambipolar diffusion for all altitudes under 260,000 ft, above which diffusion is the predominant mechanism. On the other hand, attachment is found to be considerable in all cases if the high values for ζ measurement in drift tubes are adopted. It is pointed out that during an actual re-entry much lower attachment rates will be observed; this is because drift measurements disturb the gas very little, whereas during actual re-entry the air is disturbed considerably. Electron profiles for characteristic lengths of 1 cm, 5 in., and 5 ft at a velocity of 25,500 ft/sec have been calculated for a re-entry example.[13] Comparisons are made with the attachment mechanism suppressed. The absence of this mechanism alters significantly the electron concentrations, especially

at the lower altitudes where the dependence of N_a is felt more strongly in the diffusion equation.

THE PRESENCE OF TURBULENCE

In Ref. 14 the problem of the hydrodynamic stability of a Gaussian velocity profile in an incompressible viscous wake is analyzed by using the method of Galerkin for the solution of the Sommerfeld–Orr equation. It is found that the critical Reynolds number for antisymmetric perturbations begins to develop at the value 19 with the Reynolds number defined from the relation

$$\overline{(Re)}_{crit} = \frac{U_\infty dC_D}{\nu \sqrt{2\pi}}$$

where d is defined as the effective cross–sectional dimension of the body causing the viscous wake.* The experiments of Ref. 15, undertaken for wakes behind cylinders, confirm the findings of the theory. Kovasznay[15] made his measurements in the low–Reynolds–number range and observed that the familiar Kármán vortex streets appear only above Re = 40 and that they remain stable and regular for Reynolds numbers below 160. In Roshko's paper,[16] wakes were observed for Reynolds numbers between 40 and 10,000. His experimental results coincide with Kovasznay's for Reynolds numbers between 40 and 150 where he observed that the free vortices move downstream, decaying by the laminar viscous mechanism. For Reynolds numbers greater than 300 the vortices diffused downstream turbulently and the wake became fully turbulent in about 40 to 50 diameters downstream. The region of

*Symmetric perturbations exhibit instability at $(Re)_{crit} \approx 55$; the regular Reynolds numbers are about twice as high.

Reynolds numbers between 150 and 300 was a transition range in which irregular velocity fluctuations occurred.

No experiments are available in the case of three-dimensional bluff bodies at hypersonic speeds, hence the extent of the influence of three-dimensional and compressibility effects in the development of turbulence inside the viscous wake remains unknown.

On the other hand, from elementary wake theory it is known that the effective width of the wake increases in the direction of flow x with a power between 1/2 and 1/3 for two-dimensional and circular wakes, respectively. This means that if the wake contains a small amount of the total energy, as is the case for thin boundary layers (low altitudes), the spreading of the turbulent regime towards the outside in the laminar region E of Fig. 1 will not cause significant change in the trail lengths computed by considering laminar flow. Conversely, at higher altitudes where a considerable portion of the energy associated with the moving body will go through a thick boundary layer, turbulence will spread rather rapidly, and the results of any laminar calculation will give a trail length much longer than the actual one. It should be emphasized that there is no unique definition of the trail length. Depending on the chosen observable, it may be defined as the distance behind the body at which a given instrument is unable to discriminate or record from ambient conditions.

In Ref. 6 a calculation is performed for the turbulent trail. The velocity and enthalpy profiles corresponding to station $x = x_o$ were estimated by assuming an elliptical shock wave and an isentropic expansion to atmospheric pressure along each streamline. The semiempirical eddy-diffusivity theory for the calculation of the turbulent shear was used,

based on the work of Townsend.[17] It was assumed, furthermore, that the entire trail becomes turbulent immediately after the station $x = x_o$; the trail is therefore found to be much shorter than the laminar one as computed by Feldman[1] for the same flight conditions (60,000-ft altitude and 17,500-ft/sec velocity). For the reasons explained previously, the assumption of turbulence in every streamline does not seem to be realistic, especially for the low altitude chosen in the numerical example.*

Equilibrium turbulent calculations have also been performed by Long and reported in Ref. 5. A wide range of conditions is covered with altitudes between 150,000 and 250,000 ft and velocities ranging between 15,000 and 25,000 ft/sec. The geometry chosen was a spherically blunted 10-deg cone. A turbulent Prandtl number of unity was assumed. It appears that, as in Ref. 6, turbulence has been assumed to prevail both in the viscous wake and the trail. Boundary-layer effects, however, have been neglected.

*In a later publication W. W. Short and A. Hochstim have retracted this assumption. See The Effect of Additives in the Turbulent Wake of a Re-Entry Vehicle, Convair, Physics Section Ph-087-M, August 1960.

III. APPROXIMATE UNIVERSAL SOLUTIONS

The solutions presented in the literature and discussed in the previous section have been obtained partially through numerical calculations performed by digital computers. Given a certain geometry and flight conditions, a numerical answer is provided on the nature of the trail without an intimate knowledge of the basic coupling mechanism of the different parameters involved. These parameters remain buried inside the numerical computations, and it is impossible to retrieve them in a clear form from the final result.

In this section an attempt is made to present the problem of the hypersonic trail from a fundamental point of view by using expressions in closed form, where their physical significance is more apparent. It will be shown that the closed-form results are very close to the ones predicted by machines.

THE EXPANSION PART OF THE TRAIL

We first consider the case of hypersonic trails in thermodynamic equilibrium. We shall assume, in the light of the discussion in the previous sections, that no other irreversibility is present in the flow, except for the detached shock wave ahead of the body. Let the shape of the shock wave be given by an expression of the form $R = R(x)$, the function R being continuous and admitting a first-order derivative. We are interested in calculating the ratio h/h_∞ at the station $x = x_o$ where the pressure at all values of r (see Fig. 1) and all $x \geq x_o$ is equal to the ambient pressure p_∞. From Ref. 18 we can use the isentropic exponents related to

real-gas effects in the temperature range of 3000 to 8000°K.* The following sequence of equalities is self-explanatory.

$$\frac{h_{x_o}}{h_\infty} = \frac{h_{x_o}}{h_s} \cdot \frac{h_s}{h_\infty} \cong \left(\frac{T_{x_o}}{T_s}\right)^{1/\alpha'} \left(1 + \frac{\gamma - 1}{2} M_\infty^2 \sin^2 \delta\right)$$

$$= \left(\frac{p_{x_o}}{p_s}\right)^{(\gamma' - 1)/\alpha'\gamma'} \left[1 + \frac{(\gamma - 1)}{2} M_\infty^2 \sin^2 \delta\right]$$

$$= \frac{1 + \left(\frac{\gamma - 1}{2}\right) M_\infty^2 \sin^2 \delta}{\left(\frac{2\gamma}{(\gamma + 1)} M_\infty^2 \sin^2 \delta - \frac{\gamma - 1}{\gamma + 1}\right)^{(\gamma' - 1)/\alpha'\gamma'}} \qquad (1)$$

The coefficients α' and γ' are given in Ref. 18** once the value of the entropy immediately behind the shock wave has been established. The value of an effective γ for the jump across the shock wave can be estimated by using the tables of Ref. 11 or Ref. 19. The parameter δ is the shock angle as indicated in Fig. 1, and can easily be calculated by the given equation for the shock wave

$$\sin^2 \delta = \frac{1}{1 + 1/\tan^2 \delta} = \frac{1}{1 + 1/(dR/dx)^2} \qquad (2)$$

Up to this point, we have not used the hypersonic approximations valid

---

*From a Mollier chart we can easily see that this is the range of temperatures behind the shock wave for all flight conditions of interest in re-entry.

**In Ref. 18 the symbol α instead of α' is used. In this memorandum we reserve α for later use.

for strong shock waves. Equation (1) gives, in closed form, the initial enthalpy profile at the station $x = x_o$ once the shape of the shock wave, the altitude, and flight velocity are given. Let us consider the class of shock waves given by power laws of the form*

$$R = kx^m \tag{3}$$

It is well known that such dependence suggests itself from a generalization of blast-wave theories.[20,21] (Experimental data also yield relations of this kind.[22,23]) Equation (2) becomes

$$\sin^2 \delta = \frac{1}{1 + \dfrac{R^{2(1-m)/m}}{m^2 k^{2/m}}} \tag{4}$$

In the hypersonic approximation and for all values of R smaller than the value for which the normal Mach number $M_\infty \sin\delta$ is strong enough to justify the omission of unity from the numerator and the quantity $(\gamma-1)/(\gamma+1)$ from the denominator of Eq. (1), we have

$$\frac{h_{x_o}}{h_\infty} = \frac{\left(\dfrac{\gamma-1}{2}\right)\left(\dfrac{\gamma+1}{2\gamma}\right)^{(\gamma'-1)/\alpha'\gamma'} (M_\infty^2)^{1-\frac{\gamma'-1}{\alpha'\gamma'}}}{\left[1 + \dfrac{R^{2(1-m)/m}}{m^2 k^{2/m}}\right]^{1-\frac{\gamma'-1}{\alpha'\gamma'}}} \tag{5}$$

*A body radius of one unit is assumed in these calculations throughout.

In general

$$\bar{h} \equiv \frac{h_{x_o}}{h_{x_o}{}_{R=0}} = \frac{1}{\left[1 + \frac{R^{2(1-m)/m}}{m^2 k^{2/m}}\right]^{1/\gamma_L}} \tag{6}$$

where

$$\gamma_L \equiv \frac{\alpha'\gamma'}{\alpha'\gamma' - \gamma' + 1} \tag{7}$$

From Eq. (6) it is seen that the nondimensional quantity $\bar{h}$ can be estimated with acceptable accuracy, provided we know exactly the shape of the shock wave (m and k). The enthalpy $(h_{x_o})_{R=0}$ can always be estimated directly from a Mollier chart[11] rather than through M_∞ and γ.

From the data of Ref. 18, the quantity γ_L, defining an equivalent ratio of specific heats for the isentropic expansion up to the station $x = x_o$, is computed as follows:

S (cal/gm °K	γ_L
2.4	1.22
2.6	1.20
2.8	1.19
2.9	1.18
3.0	1.18

Between the same range of entropies, corresponding to the range between 3000 and 8000°K, the coefficient α' varies by about 20 per cent, and the coefficient γ' by about 5 per cent, whereas γ_L varies by only 3.3 per cent. In other words, γ_L is independent of flight conditions.

Let us now examine in more detail the case of a blunt nose followed by a cylinder, for which it is well known that the shape of the shock is given by a parabola

$$R = k\sqrt{x} \sim \left(\frac{\pi}{2} C_D\right)^{1/4} \sqrt{x} \tag{8}$$

Substitution of Eq. (8) into Eq. (6) gives (for m = 1/2)

$$\bar{h} = \frac{1}{\left(1 + \frac{4R^2}{k^4}\right)^{1/\gamma_L}} \tag{9}*$$

It is well known from blast-wave theory that the coefficient k is directly proportional to the fourth root of the drag coefficient.[20] From experimental and theoretical calculations over a wide range of configurations, with drag coefficients varying between 0.037 and 1.37, Ref. 23 suggests the following correlation for hypersonic flow in air

$$\frac{R}{d} = 0.98 \left(\frac{x}{d}\sqrt{C_D}\right)^{0.46} \tag{10}$$

where, it will be remembered, C_D represents the nose form drag (i.e., not base drag and skin friction).

The experimental points for air from the above reference are shown in Fig. 3, along with a sketch of the different configurations tested. In the present analysis we prefer to use the correlation

$$\frac{R}{d} = 0.90\, C_D^{1/4} \left(\frac{x}{d}\right)^{1/2} \tag{11}$$

Besides the fact that the square root of x is suggested by the theory, the above relation does not lack accuracy when compared with Eq. (10). When R and x are referred to the characteristic radius r_o, the coefficient k

*Note the strong dependence of $\bar{h}$ on the numerical value of k.

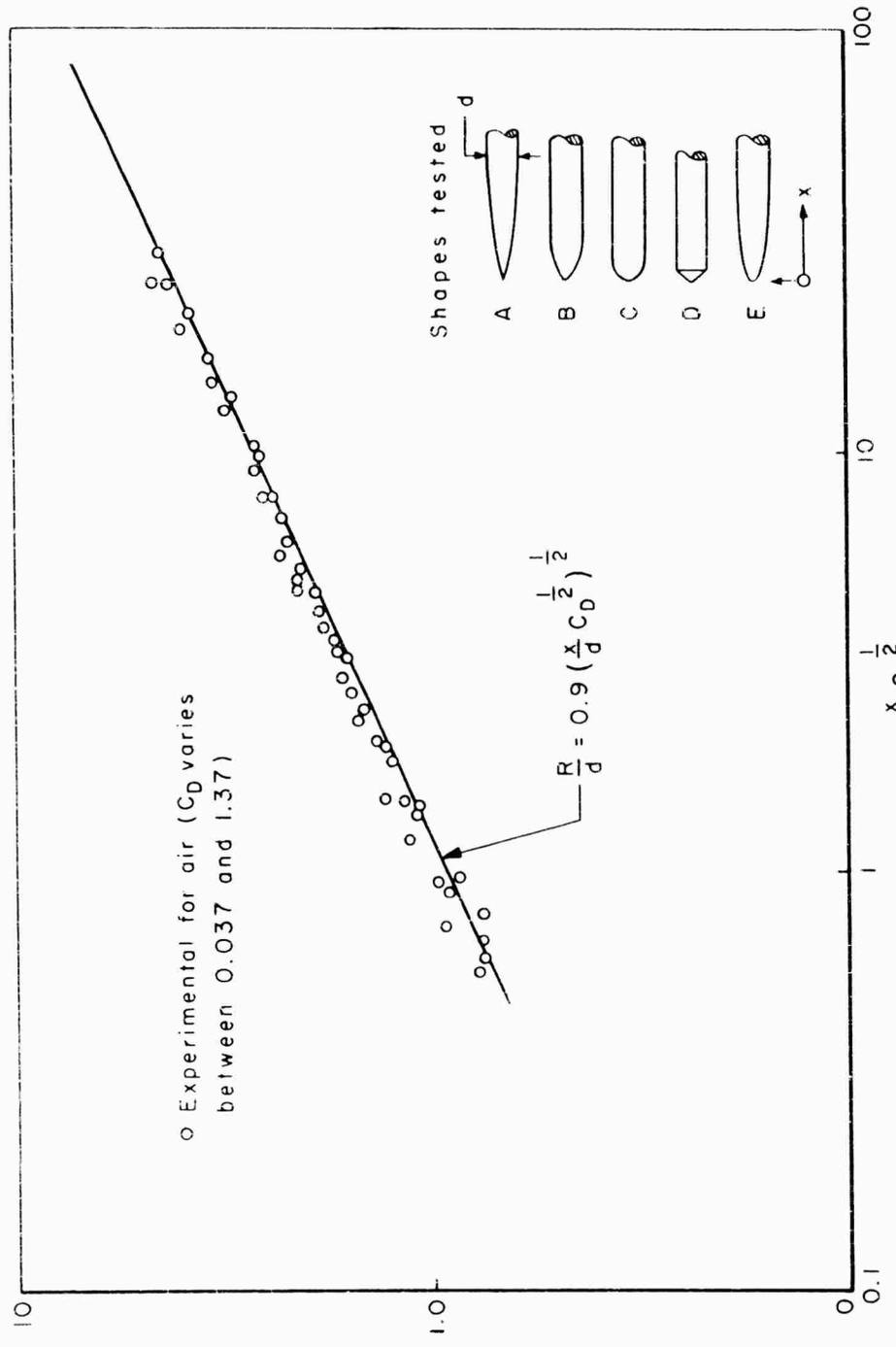

Fig. 3—Experimental data of hypersonic shock shapes correlated in accordance with the blast wave therory

takes the value

$$k = 1.27\, C_D^{1/4} \tag{12}$$

It is worth mentioning that for an altitude of 100,000 ft Feldman found, through the method of characteristics, a shock shape corresponding to a value k = 1.25 for all flight velocities considered. On the other hand, for the altitude of 60,000 ft and a velocity of 17,500 ft/sec, he found k = 1.4.

Equation (9) is truly an expression of a universal enthalpy profile, depending solely on the drag coefficient and the ratio γ_L, both being independent of altitude and flight velocity within the frame of hypersonic approximations. It might be of interest to note that the profile of Eq. (9) is analytically the same as the one emerging from a circular laminar jet.

The mass-continuity equation at the two stations x = 0 and x = x_o (see Fig. 1) may be written as

$$\rho_\infty U_\infty R dR = \rho_{x_o} U_{x_o} r dr \tag{13}$$

It is easy to establish that the Howarth transformation variable R_H used in Ref. 1 for the correlation of the enthalpy profiles obtained through the method of characteristics is connected with R as follows:

$$R^2 = \int_o^r \frac{\rho_{x_o}}{\rho_\infty} \cdot \frac{U_{x_o}}{U_\infty}\, dr^2 \cong \frac{U_{x_o}}{U_\infty}\, R_H^2 \tag{14}$$

Let us define*

$$f \equiv \frac{U_{x_o}}{U_\infty} \tag{15}$$

Equation (9) becomes

$$\bar{h} = \frac{1}{\left(1 + \frac{4f}{k^4} R_H^2\right)^{1/\gamma_L}} \tag{16}$$

For small values of R_H, the behavior of $\bar{h}$ is parabolic

$$\bar{h} \approx 1 - \frac{4f}{k^4 \gamma_L} (R_H^2) \tag{17}$$

It will be recalled that in Ref. 2 a Gaussian distribution of the form

$$\bar{h} = e^{-R_H^2/\beta_{x_o}} \tag{18}$$

was used as an analytic expression for the initial enthalpy profile. The solution of the conduction-controlled part of the trail through an integral method depends critically on the accuracy of the profile used in the neighborhood of $R \approx 0$. Comparing Eqs. (17) and (18) we find

$$\beta_{x_o} = \frac{k^4 \gamma_L}{4 f_{x_o\, R=0}} \tag{19}$$

The factor f defined in Eq. (15) can be easily computed from the fact that the stagnation enthalpy remains constant everywhere in the inviscid

---

*Since $f \approx 1$, the Howarth variable represents physically the shape of the shock. Since f varies between about 0.80 and 1.00, the maximum error in the approximation in Eq. (14) is about 10 per cent.

flow field. Its value at R = 0 is given by

$$f^2 \cong 1 - \frac{2h_\infty}{U_\infty^2}\left[\frac{h_{x_o}(0)}{h_\infty} - 1\right]$$

$$= 1 - \frac{2}{(\gamma - 1)\, M_\infty^2}\left[\frac{h_{x_o}(0)}{h_\infty} - 1\right] \qquad (20)$$

For altitudes between 60,000 and 100,000 ft and velocities ranging between 15,000 and 25,000 ft/sec, the value of f is almost a constant and equals 0.77. Equation (20) is in good agreement with the numerical findings of Ref. 1, where real-gas tables have been used.

The Gaussian depth as defined in Eq. (19) can now be calculated with $k = 1.27\, C_D^{1/4}$, $\gamma_L = 1.18$, and $f = 0.77$. We find

$$\beta_{xo} = C_D \qquad (21)$$

Feldman[1] has chosen $\beta \approx 1.0$ for all his computations, a value found for best fit after fairing the enthalpy curves from the method of characteristics into the interval $r < r_o$. His value is well justified by the above result, since for a hemisphere-cylinder geometry in hypersonic flow $C_D \approx 1$. In Fig. 4 several enthalpy profiles have been collected, corresponding to different flight conditions from Ref. 1. It is seen that the universal curve fits all the numerical data well, especially for low R's exhibiting at the same time the correct trend.* Feldman's Gaussian approximation is

*This curve is traced for a value of f at R = 0 of 0.77. The value of f at other points was computed by using the fact that the stagnation enthalpy remains constant. Note that for the conditions of curve 2 in Fig. 3 a value k = 1.4 is appropriate,[1] corresponding to a Gaussian depth of 1.50, incompatible with curve 2.

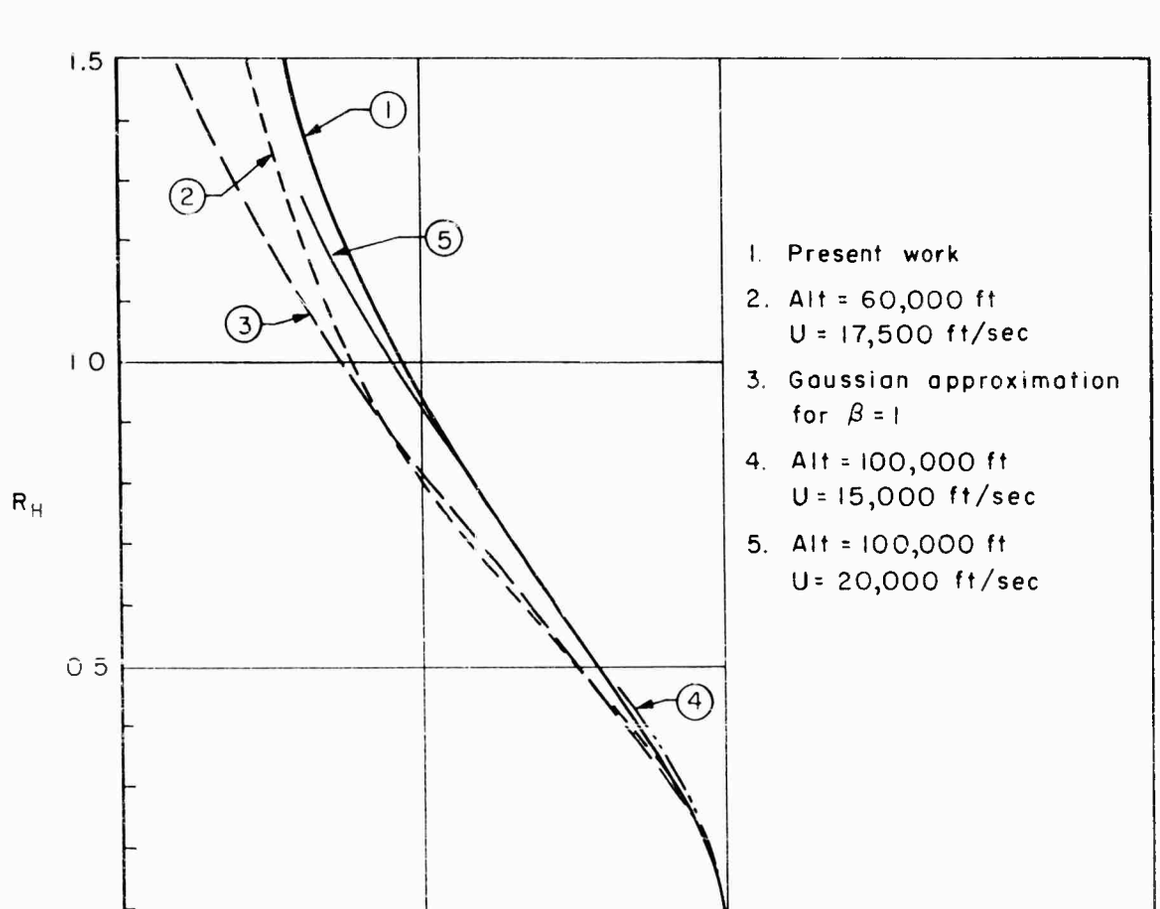

Fig. 4 — The universal enthalpy profile compared with profiles obtained by the method of characteristics in Ref. 1

also shown, and it is clear that this approximation goes to zero faster away from the axis.

The velocity-deficiency law at the section $x = x_o$ can easily be obtained by allowing ourselves the assumption of constant stagnation enthalpy in the radial direction. The statement is an exact one for adiabatic conditions with Prandtl number equal to one.

We find

$$1 - \left(\frac{U}{U_\infty}\right)^2 = \frac{2h_\infty}{U_\infty^2}\left(\frac{h}{h_\infty} - 1\right) \tag{22}$$

For $h/h_\infty >> 1$ and U/U_∞ equaling a small number compared to unity, the above is reduced to

$$\frac{\left(1 - \frac{U}{U_\infty}\right)}{\left(1 - \frac{U}{U_\infty}\right)_{R=o}} \simeq \bar{h} = \frac{1}{\left(1 + \frac{4f}{k^4} R_H^2\right)^{1/\gamma_L}} \tag{23}$$

In other words the velocity-deficiency law is exactly the same as the enthalpy law when both are referred to their value at the cross section $x = x_o$ and $R = 0$.

The method just developed can easily be applied in the case of frozen flow. As was pointed out previously, at the higher altitudes the transition point from equilibrium to frozen conditions occurs closer to the stagnation point. We may assume under these conditions that the expansion of the gas from there on takes place with a constant value γ_F calculated from either Ref. 9 or Ref. 10. Assuming that in the neighborhood of the stagnation region the shape of the shock is not altered (the value of k in Eq. (9) remains the same), the Gaussian depth $\beta(0)$ will be given by the relation

$$\beta(0) = \frac{k^4 \gamma_F}{4 f_{R=0}} \tag{24}$$

Frozen conditions have a rather small effect on the velocity;[7] therefore $\beta(0)$ will increase, since γ_F will be always greater than γ_L. On the other hand, the temperature at the station $x = x_o$ will be lower, but because of the increased Gaussian depth it will diminish in the radial direction at a slower rate. Thus, all the observables that depend on temperature will probably remain high even at large distances from the axis of the trail. The significance of this behavior must not be overlooked. We have

$$\frac{\beta_F(0)}{\beta_E(0)} = \frac{\gamma_F}{\gamma_L} \approx 0.85\ \gamma_F \tag{25}$$

As an example, consider the case of flight at an altitude of 100,000 ft and flight velocity of 20,000 ft/sec. Under these conditions Ref. 11 gives a compressibility factor behind the normal shock of 1.38 and hence an atom concentration of 0.38. From Ref. 9 we calculate for this concentration a value of $\gamma_F = 1.52$, and the same value is obtained by using the results of Ref. 10. The ratio of the two Gaussian depths for equilibrium and frozen conditions is

$$\frac{\beta_F(0)}{\beta_E(0)} = \frac{1.52}{1.18} = 1.29$$

A change of approximately 30 per cent in the degree of persistence in the radial direction of the high temperatures prevailing at the axis of the trail could be of importance for some of the observables.

Unpublished numerical calculations for frozen flow by R. Goulard verify Eq. (25).

THE LENGTH OF THE EXPANSION PART OF THE TRAIL

For the estimation of the distance x_o one can use the second-order blast-wave theory due to Sakurai[20] for the pressure decay along the distance x. We have

$$\frac{p}{p_\infty} = 0.1330 \frac{M_\infty^2}{x/r_o} + 0.405$$

Equating the above to one and solving for x_o/r_o we find

$$\frac{x_o}{r_o} \simeq \frac{M_\infty^2}{4.5}$$

The following table compares the above approximation with numerical results obtained by the method of characteristics

Altitude (ft)	Velocity (ft/sec)	$\frac{x}{r_o} = M_\infty^2/4.5$	Method of Characteristics AVCO
60,000	17,500	72	56
100,000	15,000	53	40
100,000	20,000	93	80
100,000	25,000	145	100

THE THERMAL CONDUCTION PART OF THE TRAIL

We proceed now to the calculation of the conduction-controlled part of the trail. From now on the measurement of distance x will be made from station $x = x_o$, which in the new notation will be denoted by $x = o$.

Let us define the length of the trail L as the distance from the cross section where the pressure has reached its ambient value to a point on the axis where the temperature corresponds to a given minimum ionization level. Let δ be the characteristic radius of the trail in the direction normal to the flow. Assuming that the amount of heat convected in the direction x is equal to the amount of heat conducted in direction δ, we may write

$$\rho U C_p \frac{(\Delta T)_L}{L} \sim k_t \frac{(\Delta T)_\delta}{\delta^2} \tag{26}$$

where $(\Delta T)_L$ is the temperature difference over the length L, $(\Delta T)_\delta$ is the temperature difference between the axis and the edge of the trail, and U is the characteristic velocity at the axis of the trail. On the other hand, the order of magnitude of the drag

$$\text{Drag} \sim \rho \delta^2 U^2 \tag{27}$$

or

$$\sim C_D r_o^2 \rho_\infty U_\infty^2$$

where r_o is the body radius. After introduction of the drag coefficient in the above equation, elimination of δ between Eqs. (26) and (27), and introduction of the Prandtl number, we find

$$\frac{L}{C_D r_o^2} \sim \frac{Pr}{\mu} \rho_\infty \frac{U_\infty^2}{U} \frac{(\Delta T)_L}{(\Delta T)_\delta} \tag{28}$$

The characteristic velocity U prevailing in the axis of the trail can be calculated from Eq. (20). Introduction of the factor f yields

$$\frac{L}{C_D r_o^2} \sim \frac{Pr}{\mu} \frac{\rho_\infty U_\infty}{f} \frac{(\Delta T)_L}{(\Delta T)_\delta} \tag{29}$$

The temperature ratio $\Delta T_L/\Delta T_\delta$ depends solely on the temperature at the end of the adiabatic expansion (a sole function of the flight Mach number) and the temperature corresponding to the lowest degree of ionization upon which the length L is based. Therefore we conclude from Eq. (28) that for a constant flight Mach number the length of the trail will be directly proportional to the drag coefficient, to the cross section perpendicular to the flow, and to the ambient density, which varies exponentially with altitude. It is obvious that any detailed analysis of the problem can yield no more than a numerical constant in front of the right side of Eq. (28) and the influence of the viscosity μ, which is a function of temperature. The order of magnitude of the length of the trail can be correctly estimated from Eq. (28).

We now proceed to a more detailed analysis of the problem. The energy equation, allowing for variable properties but neglecting the viscous dissipation and the components associated with the radial velocity, is

$$\rho U \frac{\partial h}{\partial x} = \frac{1}{r} \frac{\partial}{\partial r} \left(kr \frac{\partial T}{\partial r} \right) \tag{30}$$

where k is the coefficient of thermal conductivity. Following Ref. 1 we define

$$X \equiv \frac{x/r_o}{Re} = \frac{x}{r_o}\left(\frac{\mu_\infty}{\rho_\infty U_\infty r_o}\right) \tag{31}$$

Making $r_o = 1$, Eq. (30) becomes

$$\frac{\rho}{\rho_\infty}\frac{U}{U_\infty}\frac{\partial(h/h_\infty)}{dX} = \frac{1}{r}\frac{\partial}{\partial r}\left[\frac{1}{Pr}\frac{\mu}{\mu_\infty} r \frac{\partial(h/h_\infty)}{\partial r}\right] \tag{32}$$

In an integral method we need to satisfy the conditions that the total energy crossing any station x at all radii remains constant. Mathematically, we must have

$$\frac{\partial}{\partial X}\int_o^\infty \frac{h}{h_\infty} R_H dR_H = 0 \tag{33}$$

At very large distances away from the body, the velocity and enthalpy distributions will be Gaussian. On the other hand, for small distances the profiles will be of the form of Eq. (9). We choose the following enthalpy profile for the study of the conduction-controlled trail at small x

$$\frac{h}{h_\infty} \approx \frac{\alpha(x)}{\left[1 + \frac{R_H^2}{\beta'(x)}\right]^{1/\beta(0)}} \tag{34}$$

Comparison of Eq. (34) with Eq. (17) at $x = 0$ and small values of R_H gives

$$\beta(0)\beta'(0) = \frac{\gamma_L k^4}{4f_{R=0}} = \beta(0)$$

Hence, in order to approximate the initial enthalpy profile we must set $\beta'(0) = 1$.

At x = 0, Eq. (34) becomes

$$\bar{h} = \frac{1}{\left(1 + R_H^2\right)^{4f_{R=0}/\gamma_L k^4}} \tag{35}$$

Equation (35), when plotted with $f_{R=0} = 0.77$, $\gamma_L = 1.18$, and $k = 1.27$, falls slightly to the right of curve 5 and to the left of curve 1 in Fig. 4. (It is not shown there in order to avoid crowding the figure.) It constitutes a good approximation to the initial profile throughout the whole range, a property that the Gaussian distribution at the station $x = x_o$ does not seem to have. Equation (34) can now be substituted in Eq. (33); we find

$$\alpha(x)\beta'(x) = \text{const.} \tag{36}$$

We now take Eq. (32) to the limit for $R_H \to 0$. Making use of Eq. (34), we find

$$\frac{d\alpha(x)}{dX} = -\frac{4}{Pr f_{R=0}} \frac{\alpha(x)}{\beta'(x)\beta(0)} \frac{\mu(x,0)}{\mu_\infty}$$

Using Eq. (36) to eliminate $\beta'(x)$, we have

$$\frac{d\alpha(x)}{dX} = -\frac{4}{Pr f_{R=0}} \frac{\alpha^2(x)}{\alpha(0)\beta(0)} \frac{\mu(x,0)}{\mu_\infty} \tag{37}$$

Substituting Eq. (19) into the above, we find

$$\frac{d\alpha(x)}{dX} = -\frac{16}{Pr k^4 \gamma_L \alpha(0)} \frac{\mu(x,0)}{\mu(\infty)} \alpha^2(x) \tag{38}$$

The following result emerges from Eq. (38), recalling that $\sim k^4 \sim C_D$ (Eq. 8).

The gradient of the nondimensional enthalpy, calculated at the axis of the trail at the station $x = x_o$, depends only on the drag coefficient,

transport properties not considered. It is worth noting that it does not depend on the velocity deficiency at R = 0.*

Equation (38) can be integrated in a closed form provided we make the assumption of an average constant value for $\mu(x,0)$ as has already been pointed out in Ref. 1. The result is

$$\frac{\alpha(x)}{\alpha(0)} = \frac{1}{1 + \frac{16}{(Pr)k^4\gamma_L} \frac{\bar{\mu}(x,0)}{\mu_\infty} X} \tag{39}$$

From Eq. (37) it is seen that the slope of $\alpha(x)$ is inversely proportional to the Gaussian depth $\beta(0)$. For large values of x, the form of Eq. (34) should become less accurate; a Gaussian distribution will be more appropriate there.

Under the assumption of constant thermal conductivity, the heat-conduction equation (Eq. (32)) admits as an exact solution the Fourier-Bessel integral

$$h = \int_0^\infty \frac{J_o(\lambda R_H)}{\lambda} e^{-\frac{\bar{\mu}}{\mu_\infty} \frac{X}{fPr\beta_o} \lambda^2} \left\{ \int_0^\infty h(R_H,0)\ (\lambda R_H)\ J_o(\lambda R_H) d(\lambda R_H) \right\} d\lambda \tag{40}$$

Assuming as an initial condition $h(R_H,0)$ a Gaussian distribution of the form

$$h(R_H,0) = h(0,0)\ e^{-R_H^2/\beta_o} \tag{41}$$

*The Gaussian depth $\beta(0)$ from Eq. (19) was found to be inversely proportional to $f_{R=0}$.

Eq. (40) yields after integration

$$\frac{h(0,X)}{h(0,0)} = \frac{1}{1 + \frac{4\bar{\mu}}{\mu_\infty}\frac{X}{fPr\beta_o}} \; e^{-\frac{R_H^2}{1 + \frac{4\bar{\mu}}{\mu_\infty}\frac{X}{fPr\beta_o}}} \qquad (42)$$

This is the solution found by Feldman in Refs. 1 and 24 by using an integral method; however, the above arguments show that under the condition Eq. (41) it is the exact solution.

If we use Eq. (35) in conjunction with Eq. (21) as the initial condition in Eq. (40), the first integral yields[25,26]

$$\int_o^\infty \frac{h(0,0)}{(1 + R_H^2)^{1/C_D}} R_H\lambda J_o(R_H\lambda)\, d\,(R_H\lambda)$$

$$= \frac{h(0,0)\,\lambda^{\left(1 + \frac{1}{C_D}\right)} K_{\left(\frac{1}{C_D} - 1\right)}(\lambda)}{2^{\left(\frac{1}{C_D} - 1\right)} \cdot \Gamma\frac{1}{C_D}} \qquad (43)^*$$

The final result is

$$\frac{h(0,X)}{h(0,0)} = \frac{1}{2^{\left(\frac{1}{C_D} - 1\right)} \cdot \Gamma\left(\frac{1}{C_D}\right)} \int_o^\infty J_o(\lambda R_H)\, K_{\left(\frac{1}{C_D} - 1\right)}(\lambda)\, e^{-\frac{\bar{\mu}}{\mu_\infty}\frac{X}{Pr f\beta_o}\lambda^2} \lambda^{1/C_D}\, d\lambda \qquad (44)$$

Unfortunately, this last integral is not readily available in the literature in a closed form, even when $C_D = 1$, and lengthy calculations based on series expansion seem to be necessary. On the other hand, we note that

*J_o and $K_{\left(\frac{1}{C_D} - 1\right)}$ are the Bessel Functions of the first kind of order zero and modified function of the second kind of order $\left(\frac{1}{C_D} - 1\right)$, respectively.

the integral method based on Eq. (35) as the boundary condition yields the same result at the axis of the trail as the exact solution based on an initial Gaussian distribution. This of course results from the parabolic character of both distributions in the neighborhood of the axis.

We now turn our attention to the possibility of obtaining a closed-form solution for the case of variable thermal conductivity. Within the range of temperatures and pressures of interest here, the Prandtl number remains constant, whereas the viscosity still obeys Sutherland's law.* From Fig. 5 it is seen that the two suggested correlations of viscosity with enthalpy are in good agreement with the exact values for pressures between 10^{-1} and 10^{-2} atm for nondimensional enthalpies less than 100, whereas for higher enthalpies the correlations are good for pressures between 10^{-3} and 10^{-4} atm.

Assuming in general a power law for viscosity of the form

$$\mu = \mu_o \, (h/RT_o)^{\omega} \tag{45}$$

with Pr = 0.70, $k^4 = 2.62\ C_D$, and $\gamma_L = 1.20$, we find

$$\frac{h(0,x)}{h(0,0)} = \frac{1}{\left\{ 1 + \dfrac{7.25\ \mu_o\ (1+\omega)\left[h(0,0)\right]^{\omega}}{\rho_\infty\ U_\infty\ \left[RT_o\right]^{\omega}}\ \dfrac{x}{C_D r_o^{\,2}} \right\}^{\frac{1}{1+\omega}}} \tag{46}$$

For the calculations of Figs. 6 – 10 and 12, both 0.25 and 0.28 exponents were used for ω; it was found that the difference in the results was

*For altitudes up to 250,000 ft and velocities up to 25,000 ft/sec, the temperature at the axis after expansion to ambient pressure is less than 4500°K.

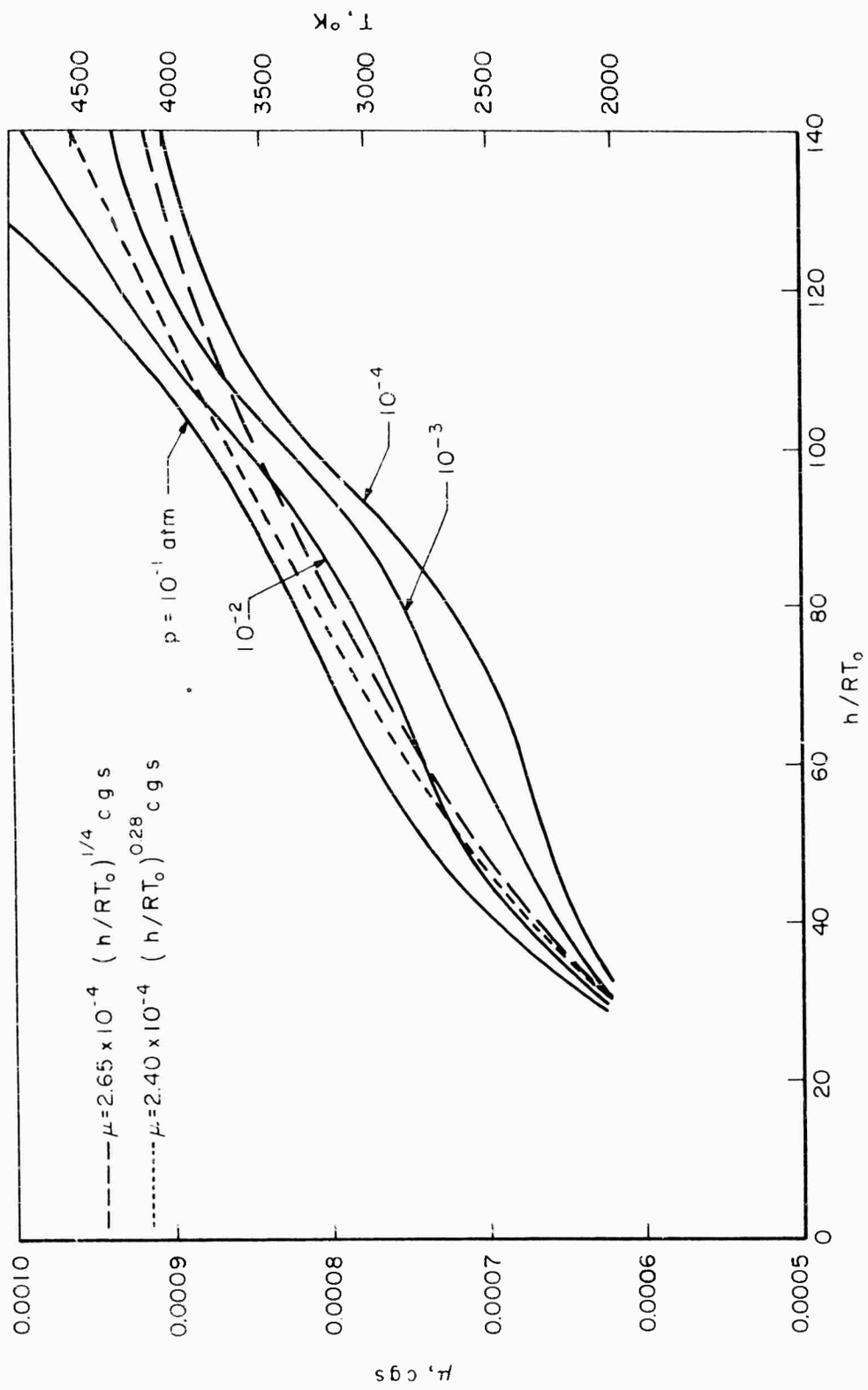

Fig. 5 — Viscosity laws as power functions of enthalpy

small. In Fig. 6, Eq. (46) is plotted for a value of $\omega = 0.25$

$$\frac{h}{h(0,0)} = \frac{1}{\left\{1 + \frac{\left[h(0,0)/RT_o\right]^{0.25}}{415\ \rho_\infty\ U_\infty}\left(\frac{x}{C_D r_o^2}\right)\right\}^{0.80}} \tag{47}$$

In Eq. (47) it is necessary to express ρ_∞ in grams per cubic cm. Figure 7 is the result of calculations based on Eq. (47) for different altitudes and velocities in terms of the electron concentration rather than the enthalpy.

We observe that for the same velocity the electron concentrations are higher for the lower altitudes, and at the same time the rate of decrease is also slower. On the other hand, for the same altitude, lower velocities correspond to lower electron concentrations with a faster rate of decay in the axial direction. For a given lower electron concentration the results of Fig. 7 may be used to plot the length of the trail versus altitude for different velocities. These calculations are shown in Figs. 8 – 10.

THE INFLUENCE OF THE TRAILING SHOCK

As was stated in the introduction, the influence of the trailing shock in the observables associated with the conduction-controlled part of the trail will be rather limited. In order to give an estimate of its importance in a closed form we make the extreme assumption that the state of the gas just before the trailing shock is such that the free-stream pressure has been reached. Some simple calculations entirely similar to the ones that led to Eq. (9) yield the following result

$$\frac{h}{h(0,0)} = \frac{1}{\left(1 + \frac{4R^2}{k^4}\right)^{\frac{1}{\gamma_L}\left(2 - \frac{1}{\gamma_L}\right)}} \tag{48}$$

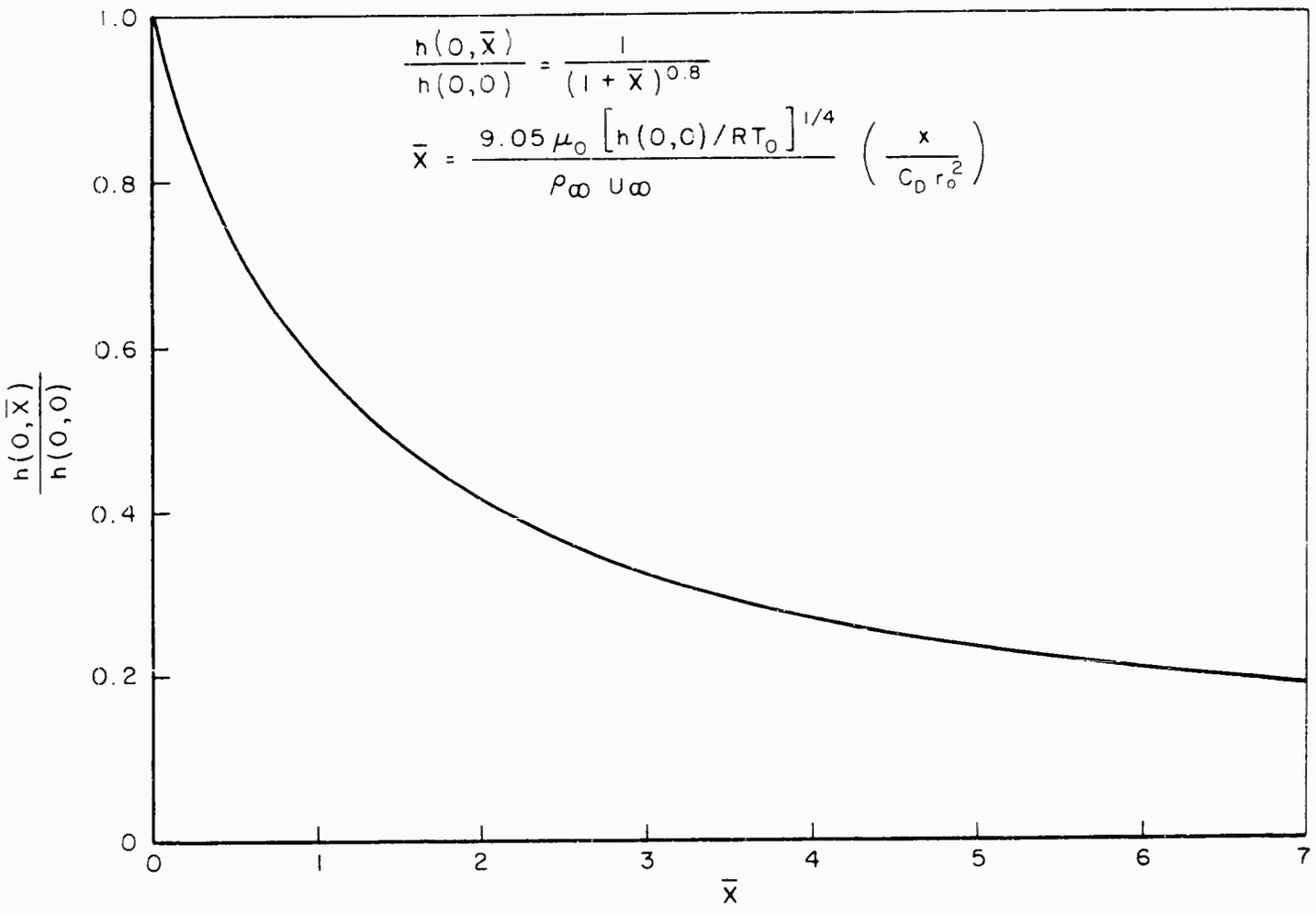

Fig. 6 — Universal solution of the conduction-controlled part of the trail with variable thermal conductivity

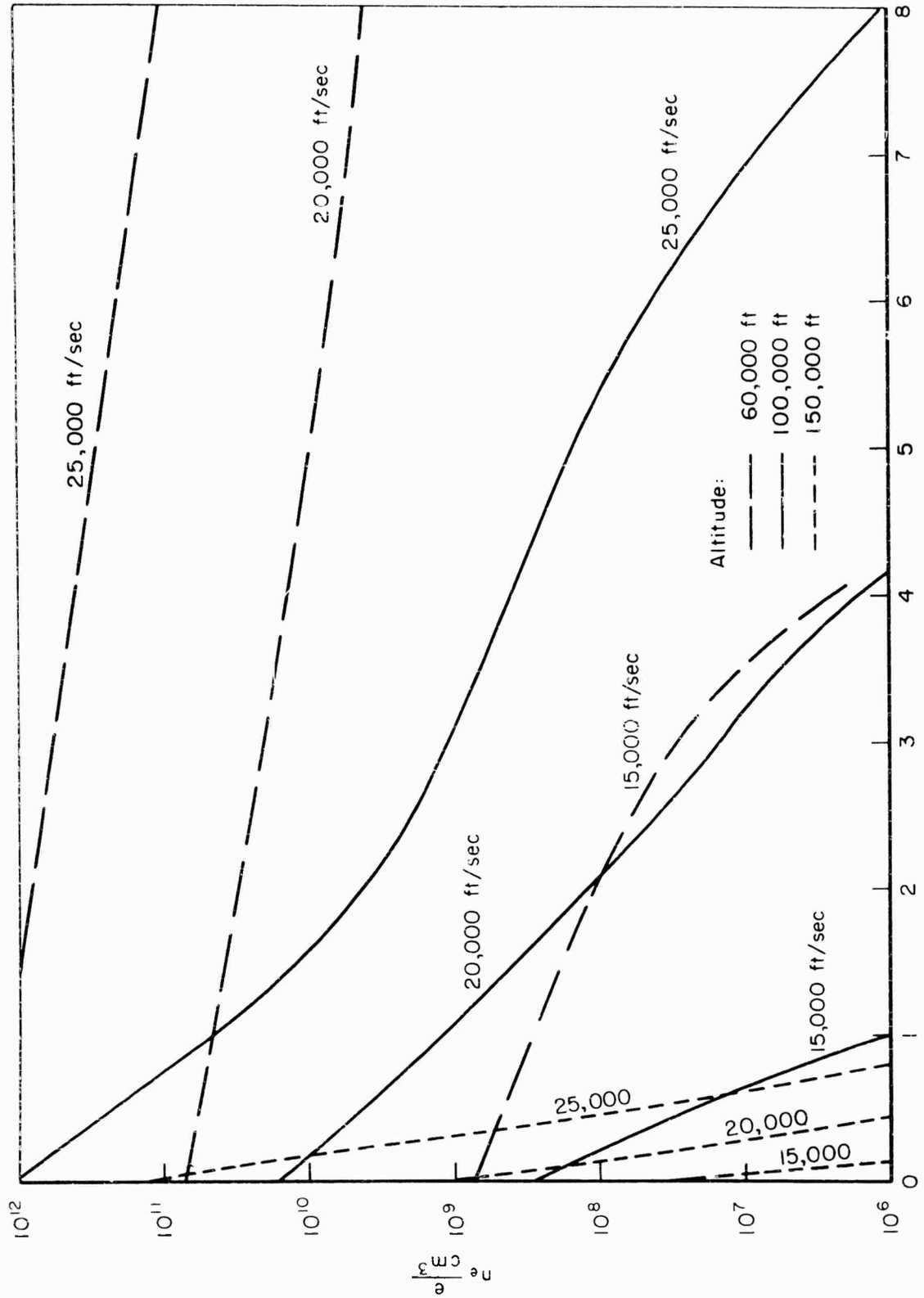

Fig. 7 — Electron-concentration decay at the axis of the ion trail for different altitudes and velocities

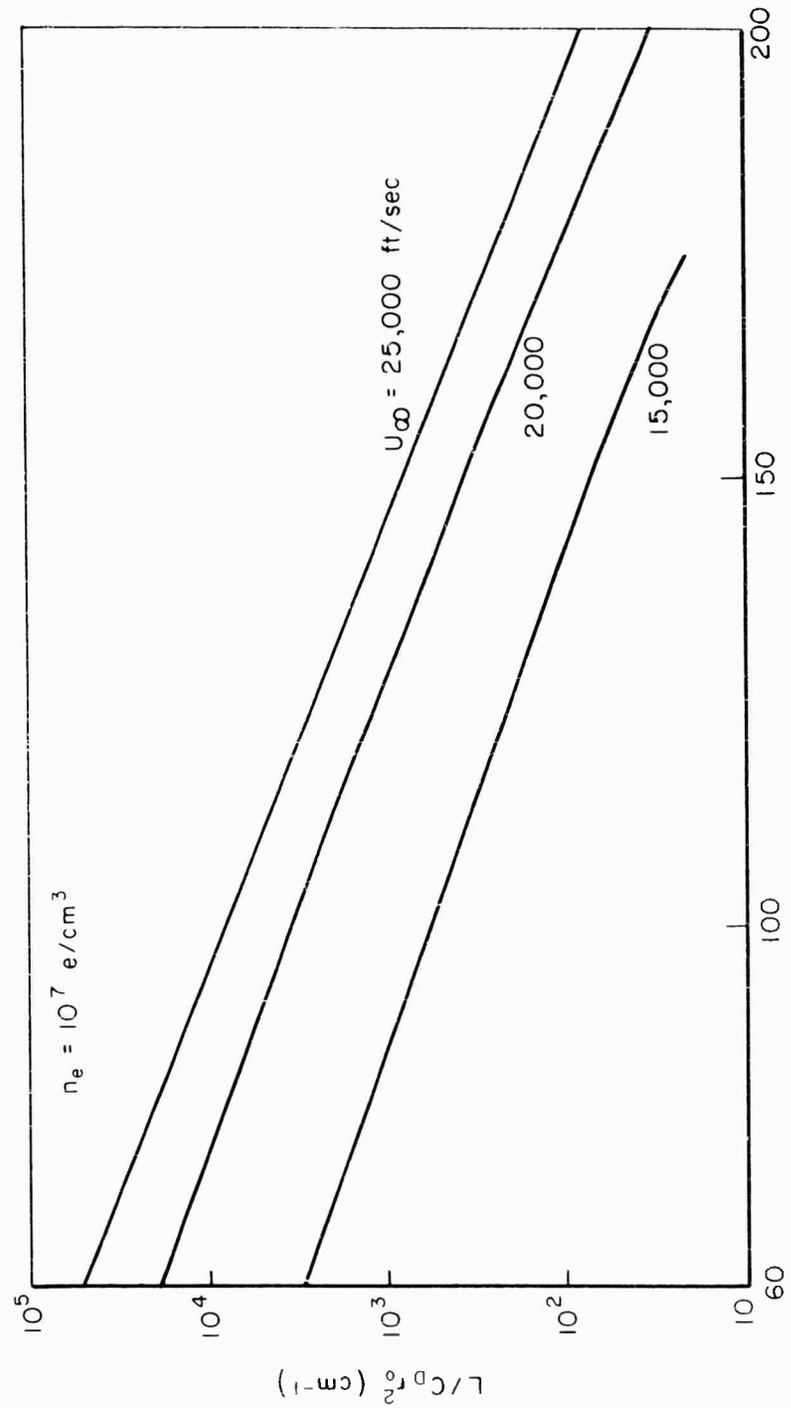

Fig. 8 — Length of the ion trail versus altitude for different constant velocities based on a minimum electron concentration of 10^7 e/cm^3

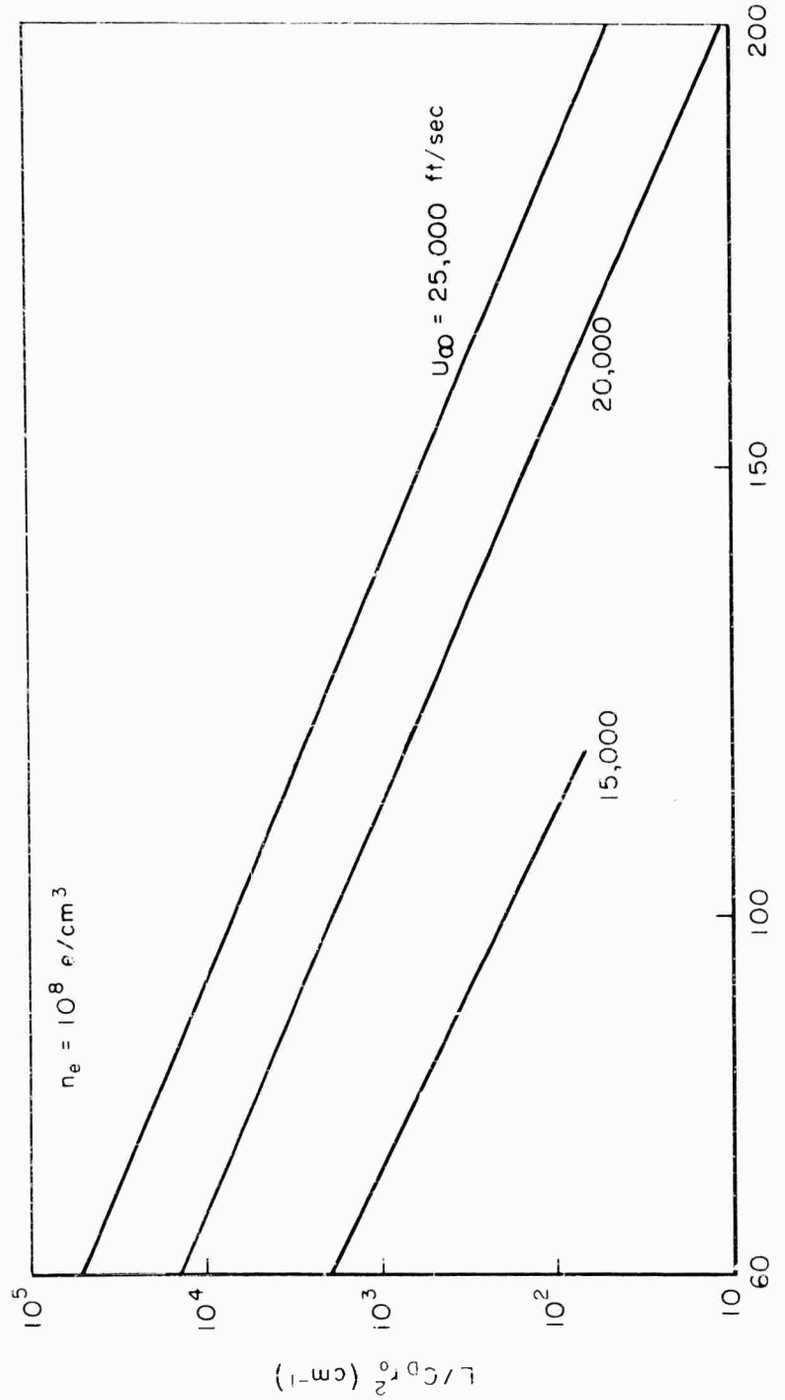

Fig. 9 — Length of the ion trail versus altitude for different constant velocities based on a minimum electron concentration of 10^8 e/cm^3

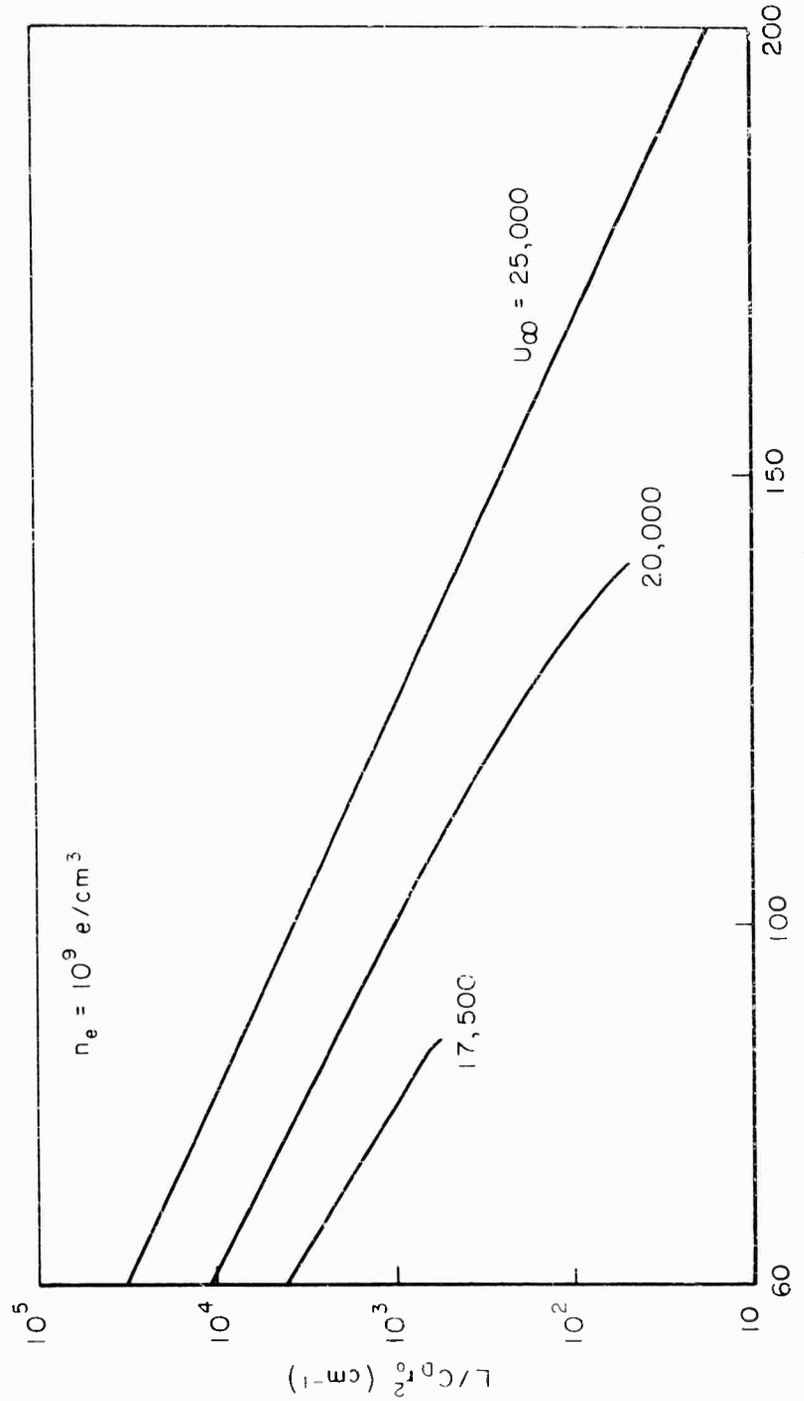

Fig. 10 — Length of the ion trail versus altitude for different constant velocities based on a minimum electron concentration of 10^9 e/cm^3

From the above we observe that the equivalent new Gaussian depth will be smaller than the one found when the trailing shock was neglected, by the factor $(2 - 1/\gamma_L)^{-1} \approx 0.86$. This means that, apart from the fact that the temperature in the center line at the end of the second expansion will be higher, these higher temperatures will persist over a smaller range in the neighborhood of the axis. Furthermore, the temperature at the axis of the trail will decay faster, since we have shown before that the rate of decay is inversely proportional to the Gaussian depth.

Figure 11 shows the extent of the influence of the second shock under the above assumptions for an altitude of 100,000 ft and three different velocities. As is evident on physical grounds, the second shock is more influential at the higher velocities where the length of the trail will be somewhat greater. In terms of the nondimensional distance X^*, as defined in Fig. 11, for the velocity of 25,000 ft/sec the difference is of the order of 17 per cent, whereas for the remaining two velocities the difference is negligible. Recalling that the above calculations correspond to rather extreme conditions, we conclude that the role of the trailing shock in the conduction part of the trail is limited.

DISCUSSION OF RESULTS

The present analysis has shown that the determination of the length of the ion trail under the assumption of thermodynamic equilibrium is controlled entirely by the shape of the bow shock wave or the drag coefficient of the object. For bluff bodies (C_D of about 0.9 or higher) boundary-layer effects will be negligible. On the other hand, for slender, long bodies these effects cannot be neglected, and therefore the present results should be understood as providing an upper limit for the length of the trail. It

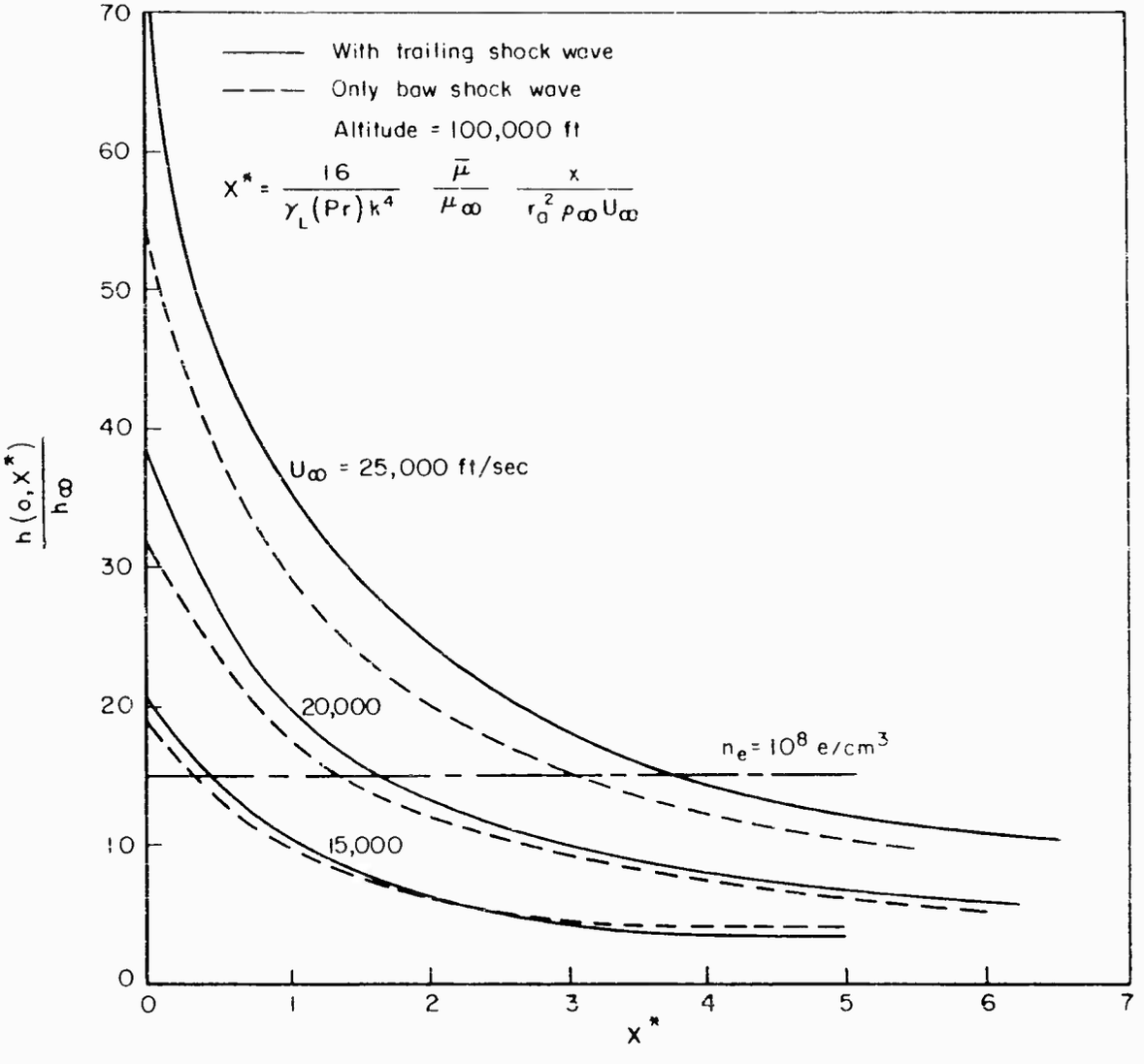

Fig.11 — Influence of the trailing shock wave in the enthalpy decay at the axis of the conduction-controlled part of the trail

should also be added that for slender but short bodies the influence of the second shock could be rather prominent.

The equilibrium solution presented in this memorandum is certainly valid for altitudes less than 150,000 ft. For high altitudes, where the assumption of frozen flow could be justified, the basic form of the equilibrium solution for the distribution of temperature or enthalpy at the cross section at the end of the adiabatic expansion can be maintained, based nevertheless on the frozen ratio of the specific heats. Solution of the problem by taking into account the exact chemistry of all the species present, including ambipolar diffusion and electron attachment in both the expansion and conduction-controlled regions, has yet to be obtained.

From Figs. 8 – 10 we observe that for constant velocities the trail length is an exponential function of altitude. As a matter of fact, the exponent is very nearly the same as the one corresponding to the density of an exponential atmosphere. If the altitude is denoted in thousands of feet, the exponent for the density variation in a simple isothermal atmosphere is about (- alt/23.5), whereas the lines in Figs. 8 - 10 correspond to exponentials equal to about (- alt/19). The steeper slope corresponding to the trail length comes about from the fact that for constant flight velocity the value of the enthalpy needed for the lowest electron concentration upon which the trail length is based is higher for high altitudes where the mass density is low. Inspection of Eq. (47) shows that the ratio $h(0,0)/h(0,L)$, apart from its dependence on the Mach number through $h(0,0)$, depends also on the altitude through $h(0,L)$, as was just explained; in this fashion the effective density exponent changes somewhat.

In Fig. 12 a plot is made of the length of the equilibrium ion trail for an actual re-entry monitored by three different frequencies corresponding to electron concentrations of 10^7, 10^8, and 10^9 electrons/cm^3. As an example, for the last electron concentration,* between the altitudes of 100,000 and 60,000 ft, we see from Fig. 12 a value for $(L/C_D r_o^2) \approx 3000$ cm^{-1}. For an object of cross section $r_o^2 \approx 100$ cm^2 with a drag coefficient of one, the length of the trail will be 3 km. For the same object at an altitude of 150,000 ft, the length will be only 200 m.

Finally we close with the remark that for given altitude, velocity, observed length of the ion trail, and the ballistic coefficient $(W/C_D r_o^2)$, use of a graph similar to the one of Fig. 12 yields the quantity $(C_D r_o^2)$, from which the weight of the re-entering object can be estimated.

---

*10^9 electrons/cm^3 correspond roughly to a frequency of 300 Mcps.

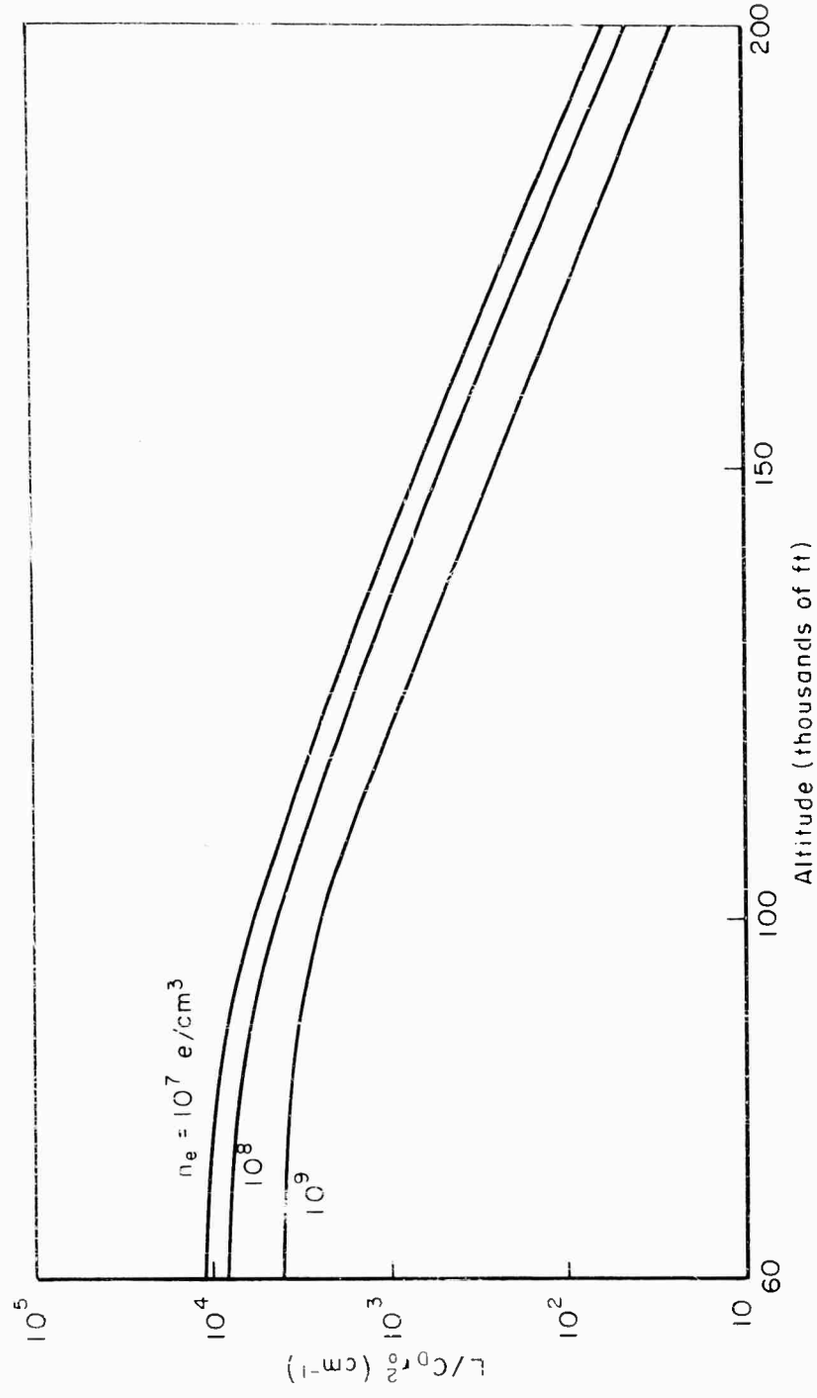

Fig. 12 — The length of the ion trail versus altitude for an illustrative re-entry and different minimum ionization levels

REFERENCES

1. Feldman, S., Trails of Axi-symmetric Hypersonic Blunt Bodies Flying Through the Atmosphere, AVCO-Everett Research Laboratory, Research Report 82, December 1959.

2. Feldman, S., A Numerical Comparison Between Exact and Approximate Theories of Hypersonic Inviscid Flow Past Slender Blunt-nosed Bodies, AVCO-Everett Research Laboratory, Research Report 71, June 1959.

3. Goulard, M., and R. Goulard, The Aerothermodynamics of Re-entry Trails, presented at the ARS Semi-annual Meeting, May 9-12, 1960, ARS Preprint 1145-60, May 1960.

4. Ting, L., and P. Libby, Fluid Mechanics of Axisymmetric Wakes Behind Bodies in Hypersonic Flow, General Applied Science Laboratories, Inc., Technical Report No. 145, March 1960.

5. Lew, H. G., and V. A. Langelo, Plasma Sheath Characteristics about Hypersonic Vehicles, Space Sciences Laboratory, General Electric Company, Report R60SD356, April 1960.

6. Short, W. W., Analytic Solution of Velocity and Temperature in an Axi-symmetric Turbulent Wake, Convair, San Diego, July 1960.

7. Bloom, M., and M. Steiger, Inviscid Flow with Non-equilibrium Molecular Dissociation for Pressure Distributions Encountered in Hypersonic Flight, presented at the IAS 28th Annual Meeting, IAS Paper No. 60-26, January 1960.

8. Bray, K. N. C., Departure from Dissociation Equilibrium in a Hypersonic Nozzle, Fluid Motion Sub-Committee, Aeronautical Research Council, March 1959.

9. Hayes, W., and R. Probstein, Hypersonic Flow Theory, Academic Press, New York, 1959.

10. Geiger, R. E., "On the Frozen Flow of a Dissociated Gas," J. Aero. Sci. Vol. 26, No. 12, December 1959, pp. 834-835.

11. Feldman, S., Hypersonic Gas Dynamic Charts for Equilibrium Air, AVCO-Everett Research Laboratory, Research Report 40, 1957.

12. Re-entry Physics Program Semiannual Technical Summary Report to the Advanced Research Projects Agency, 1 October 1958 - 30 June 1959, Lincoln Laboratory, Massachusetts Institute of Technology, October 8, 1959.

13. Re-entry Physics Program Semiannual Technical Summary Report to the Advanced Research Projects Agency, 1 July 1959 - 31 December 1959, Lincoln Laboratory, Massachusetts Institute of Technology, March 23, 1960.

14. Arkhipov, V. N., "The Formation of Streaming Fluctuations Behind a Solid Obstacle," Soviet Phys. - JETP, 1959, pp. 1117-1120.

15. Kovasznay, L., "Hot Wire Investigation of the Wake Behind Cylinders at Low Reynolds Numbers," Proc. Royal Soc. (London), A198, 1949, pp. 174-190.

16. Roshko, A., On the Development of Turbulent Wakes from Vortex Streets, NACA TN 2913, March 1953.

17. Townsend, A. A., The Structure of Turbulent Shear Flow, Cambridge University Press, London, 1956.

18. Logan, J. G., and C. E. Treanor, "Polytropic Exponents for Air at High Temperature," J. Aero. Sci., Vol. 24, No. 6, June 1957, pp. 467-468.

19. Gilmore, F. R., Equilibrium Composition and Thermodynamic Properties of Air to 24,000°K, The RAND Corporation, Research Memorandum RM-1543, August 1955.

20. Lees, L., and T. Kubota, "Inviscid Hypersonic Flow over Blunt-nosed Slender Bodies," J. Aero. Sci., Vol. 24, No. 3, March 1957, pp. 195-197.

21. Sedov, L., Similarity and Dimensional Methods in Mechanics, Academic Press, New York, 1959.

22. Mueller, J., and W. Close, An Investigation of Induced-Pressure Phenomena on Axially Symmetric Flow-Aligned, Cylindrical Models Equipped with Different Nose Shapes at Free-stream Mach Numbers from 15.6 to 21 in Helium, NASA TN D-373, May 1960.

23. Van Hise, V., Analytic Study of Induced Pressure on Long Bodies of Revolution with Varying Nose Bluntness at Hypersonic Speeds, NASA TR-R-78, Advance Copy, 1960.

24. Feldman, Saul, "On Hypersonic Wakes in the Atmosphere," (letter), Phys. of Fluids, Vol. 3, No. 3, May-June 1960, p. 479.

25. Titchmarsh, E. C., Introduction to the Theory of Fourier Integrals, Oxford Clarendon Press, London, 1948, p. 201.

26. Whittaker, E. T., and G. N. Watson, A Course of Modern Analysis, Chambridge University Press, London, 1944, p. 385.